Fatiga a Alta Temperatuta y Carga con Amplitud Variable de Acero Inoxidable 235MA

Carmen Madrigal Sánchez

Universidad de Sevilla

Escuela Técnica Superior de Ingenieros Industriales

Director: Dr. Alfredo Navarro Robles

April,2006

Este proyecto fin de carrera se basa en el trabajo realizado por la autora en condición de *Master Thesis* en la Universidad de Lund (Suecia), bajo el título:

High Temperature Low Cycle Fatigue Testing under Variable Amplitude Loading for 235MA

Lunds Tekniska Högskola

Lunds Universitet

Sweden

November, 2005

Author: Carmen Madrigal

Supervisor: Michael Andersson

Examiner: Christer Persson

Abstract

The main goal of this project was the startup and readjustment of the fatigue testing equipment, available at the division of Material Sciences at LTH. In order to reach this aim, high temperature low-cycle variable-amplitude fatigue testing on stainless steel grade 253MA was implemented on stainless steel, grade 253MA. A research on the accuracy of Palmgren-Miner rule for cumulative damage predictions was carried out. The experimental data showed the acceptable performance of this law which remained conservative for most samples. Alternative constant amplitude curves (S-N curve) were proposed concluding that the Total Strain approach described the experimental data better than the Coffin-Manson relationship. The effects of switched test sequence, prolonged relative duration of blocks and peak loads were simultaneously analyzed.

Acknowledgments

I would like to extend profound thanks to the division of Material Science at LTH for giving me the chance to write this paper under its supervision. To Christer Persson, examiner of this thesis, for his dedication and contributions of time and expertise. Special thanks to my supervisor Michael Andersson, without his help, this document would not exist.

Lund, November 2005

Contents

1. Introduction

1.1. Background

High temperature operating requirements for equipment have drastically increased over the past 20 to 30 years [1]. In a notorious number of applications the higher the temperature, the greater the efficiency of the processes.

Fatigue is present in most of these uses. This might be very dangerous as a conventional stress analysis probably would lead to an assumption of safety that does not exist [2].

Furthermore, real life situations are rarely under constant amplitude loading. In most cases, the amplitude of the load is varying. Startups, stops, overloads, speed switches and so on, are examples of variable amplitude fatigue.

Palmgren-Miner relation is the simplest available method to analyze this problem. However, different studies show the inaccuracy of its predictions [3, 4].

All these considerations make of this topic an interesting and important field of research, with direct applications in the nowadays industry.

1.2. Objectives

The testing equipment for low cycle fatigue at high temperatures in the Material Science division of *Lunds Tekniska Högskola*, LTH, had been recently set up to

perform low cycle fatigue testing of a certain stainless steel grade. The tuning had been carried out as a Master Thesis developed by Borg [5] who verified Coffin-Manson relation for constant amplitude load fatigue testing.

The division wanted to go one step further and elaborate a study on variable amplitude fatigue testing. In order to achieve this goal, a second Master Thesis was proposed and accomplished. Verification of Palmgren-Miner cumulative damage law was the main objective of the study.

Furthermore, the influence of several factors on the material behaviour was a secondary analysis of interest. Load peaks, relative block durations and sequence of loading were the main factors considered in this investigation.

This report describes into detail the whole research process. A first theoretical section provides the reader with a basis for deeply understanding the methods, deductions and decisions taken throughout this work. A minute description of the experimental preparation, the equipment setting and the implementation of the experiments follows in the third section. The results are finally presented and analyzed leading to some interesting conclusions at the end of the document.

2. Theory

2.1. High temperature materials

High temperature operating requirements for equipment have drastically increased over the past 20 to 30 years. Engineering applications are widely used in the world industry and continuously developed in different businesses such as the utility, aircraft, and chemical industries. [1]

Therefore, the quest of materials that can withstand these high temperatures is a need in nowadays research. The requirements of endurance and performance at different ranges of temperature vary depending on the purpose of the device. However, good behaviours at both low and high temperature is a must in many cases.

In the power-generation industry, in order to extract useful work from a fuel, it must first be burned so as to bring some fluid (usually steam) to high temperatures. Thermodynamics indicates that the higher the temperature, the greater the efficiency of the conversion of heat to work.

As a matter of fact, high temperature materials are also a part of daily life. Tungsten, what the filaments of light bulbs are made of, is a very representative high temperature material used in controlled environments. Environment plays an important role in these uses as it controlls time-dependent processes responsible for fracture, in general, thermally activated. The thin string might reach 2500 ℃ in use, however, the stresses the filament undergoes are due to its own weight and to the thermal stresses caused by the heat. [6]

Extremely more complicated is the case of the failure of some components of aircraft engines where cyclic loads at elevated temperatures are involved [7]. In a gas turbine aero engine, the compressor disc and casing are subjected to high strain fatigue at 400 ℃, the combustor liner to thermal fatigue at 982 ℃. The turbine discs are susceptible to high strain fatigue and creep in the temperature range of 371–649 ℃ and the turbine blades undergo thermomechanical fatigue, high-cycle fatigue and/or stress rupture, at temperatures of up to 982 ℃.

It is readily seen from these examples that high temperature materials is a topic of major concern. Nevertheless, the complexity of the interactions between cyclic loads, creep and environmental corrosion is still far from known.

2.2. Fatigue

Fatigue, as Roylance claims [2], is a process in which damage accumulates due to the repetitive application of loads that may be well below the yield point. The process might be very dangerous as a conventional stress analysis probably would lead to an assumption of safety that does not exist.

According to Suresh [7], the first study of metal fatigue is believed to has been carried out by the German engineer W.A.J. Albert around 1829. Ever since, interest in the subject began to expand with the increasing use of ferrous structures and the consequent unexpected catastrophic failures resulting in the loss of human lives.

2.2.1. Different approaches to fatigue

Historically, fatigue has been tackled from two different approaches: *total-life* versus *defect-tolerance* [7]. *Total fatigue life* is characterized in terms of stress or strain range. In this method, the specimen is initially uncracked and the number of stress or strain cycles necessary to initiate and propagate the fatigue crack until failure indicates the fatigue life.

On the other hand, fracture mechanics introduces a *defect-tolerant* approach, where the specimen is considered flawed *a priori* and fatigue life is defined as the number of cycles to propagate the dominant crack from its initial size to some critical dimension.

The procedures could apparently provide contradictory guidelines to design for optimum fatigue resistance. These discrepancies can be reconciled by noting that the former deals with the resistance to crack initiation while the latter is based on the resistance to fatigue crack growth. Design philosophy for a specific application dictates the choice between both trends. A trade-off between both recommendations is often required though.

Total-Life approaches. Phenomenological continuum approaches are widely used to characterize total fatigue life as a function of the applied stress range, strain range, mean stress and environment. These stress- or strain-based methodologies embody the damage evolution, crack nucleation and crack growth stages of fatigue into a single, experimentally characterizable continuum formulation [7].

The German engineer Wöhler was the precursor of the stress-life approach,

introducing in 1860s the concept of "endurance limit", which characterizes the applied stress amplitude below which a material is expected to have an infinite fatigue life, Figure 2.1. Applications where low-amplitude cyclic stresses induce primarily elastic deformation in a component which is designed for long life, so-called *high cycle fatigue* (HCF), are the main fields of use for this formulation. The expression relating the stress amplitude, $\sigma_a = \Delta\sigma/2$, in a fully-reversed, constant-amplitude fatigue test to the number of load reversals to failure, $2N_f$, is

$$\frac{\Delta\sigma}{2} = \sigma_a = \sigma_f^{'}(2N_f)^b, \tag{2.1}$$

where $\sigma_f^{'}$ is the fatigue strength coefficient and b is known as the fatigue exponent or Basquin exponent.

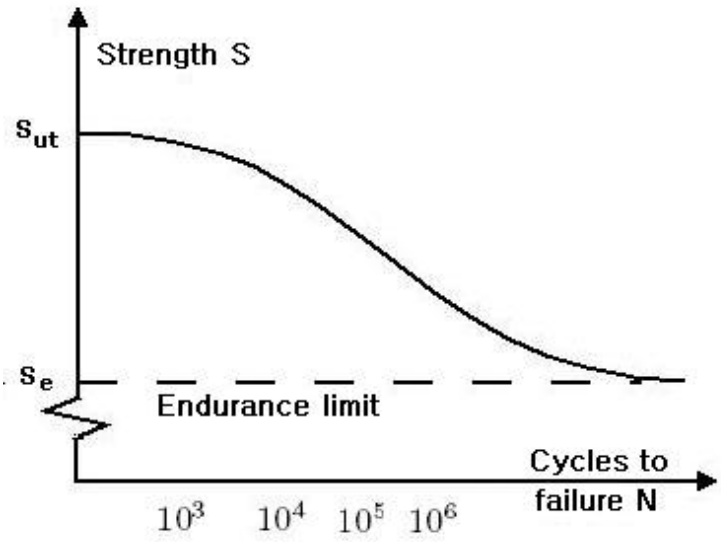

Figure 2.1: Typical Wöhler or S-N diagram showing the variation of the stress amplitude for fully reversed fatigue loading as a function of the number of cycles to failure.

Conversely, considerable plastic stress amplitudes or stress concentrations noticeably shorten fatigue life, leading to *low cycle fatigue* (LCF), where the role of the plastic strain is taken into consideration. Coffin (1954) and Manson (1954)

independently proposed a characterization of LCF based on the plastic strain amplitude.

They noted that when the logarithm of the plastic strain amplitude, $\Delta\epsilon_p/2$, was plotted against the logarithm of the number of load reversals to failure, $2N_f$, a linear relationship resulted for metallic materials, i.e.

$$\frac{\Delta\epsilon_p}{2} = \epsilon'_f(2N_f)^c, \tag{2.2}$$

where ϵ'_f is the fatigue ductility coefficient and c is the fatigue ductility exponent. Moreover, Coffin-Manson relationship, equation 2.2, could also be used to characterize the total fatigue life noting that the total strain amplitude is the sum of elastic and plastic strain amplitudes. Thus, combining equations 2.1 and 2.2 with the Hook's Law one obtains:

$$\frac{\Delta\epsilon}{2} = \frac{\sigma'_f}{E}(2N_f)^b + \epsilon'_f(2N_f)^c. \tag{2.3}$$

Figure 2.2 shows the variations of the elastic, plastic and total strain amplitude as functions of the number of load reversals to failure, $2N_f$.

Damage-tolerant approach. As discussed earlier, the other branch of the modern designs is based on the premise that engineering structures are inherently flawed. Therefore, the rate of growth of a fatigue crack is the main concern in this theory. Such rate of growth of a fatigue crack subjected to cyclic stresses, expressed in terms of the crack length increment per cycle, $\mathrm{d}a/\mathrm{d}N$, is characterized by the stress intensity factor range, $\Delta K = K_{max} - K_{min}$, by the power law relationship so called Paris law, equation 2.4.

$$\frac{\mathrm{d}a}{\mathrm{d}N} = C(\Delta K)^m, \tag{2.4}$$

where C and m are scaling constants.

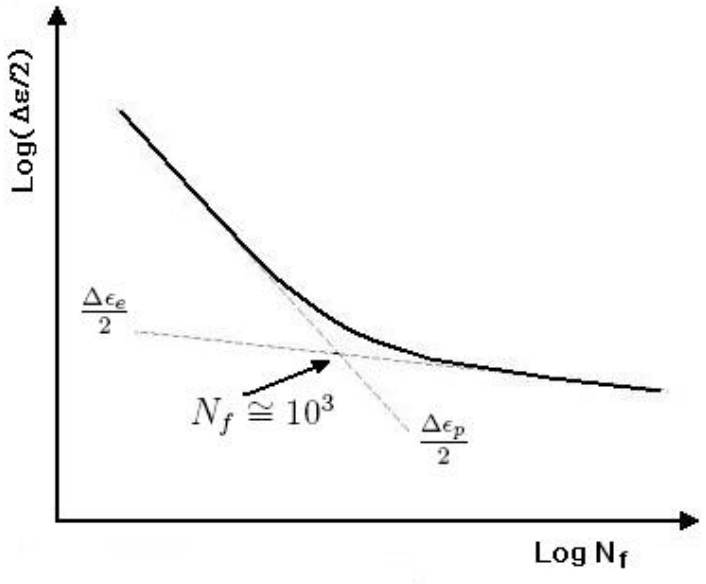

Figure 2.2: Elastic, plastic and total strain amplitude versus the number of load reversals to failure $2N_f$.

The stress intensity factor describes the stresses in the vicinity of a crack edge and is determined by equation 2.5

$$K = Y\sigma\sqrt{\pi a}, \tag{2.5}$$

where Y is a geometrical factor, σ represents the stresses and a is the crack length.

Three regimes of fatigue crack growth can be distinguished in Figure 2.3, where the Paris power law relationship has been plotted. It can be appreciated that the linear variation which pertains to stable fatigue fracture appears over only a portion of the total crack growth resistance curve. At extreme values of ΔK, there is a precipitous rise in crack growth rates with increasing ΔK. The first regime is associated with the existence of a threshold stress intensity factor range ΔK_0. Below this threshold the cracks either remain dormant or their growth rate is undetectable. The second regime is referred to as Paris regime which presents a linear variation described by equation 2.4. The last regime pertains to the

range of high ΔK values where crack growth rates increase rapidly causing catastrophic failure.

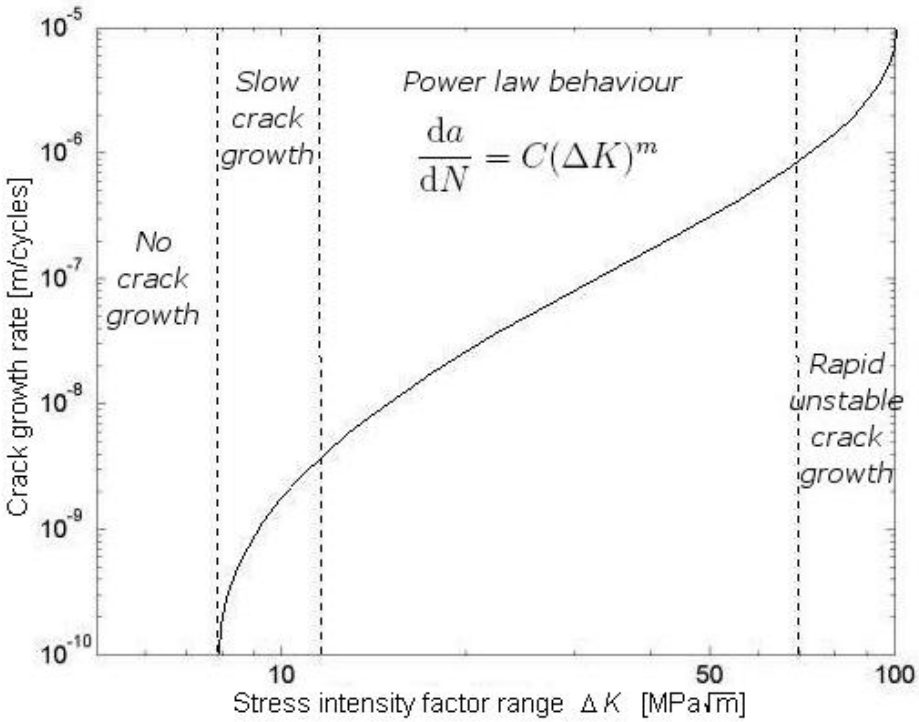

Figure 2.3: Stable fatigue crack propagation.

2.2.2. Cyclic deformation. Work hardening and softening

When a material is subjected to cyclic load, the stress-strain curve takes the form of a loop. Figure 2.4(a) shows a typical hysteresis loop where the parameters used to describe its salient features are defined.

The uniaxial deformation of engineering alloys subjected to cyclic loads is typically associated with a transient phenomena illustrated in Figure 2.5. In the case of constant-amplitude stress-controlled loading, the cyclic hardening or softening of the material is reflected by a reduction or an increase, respectively,

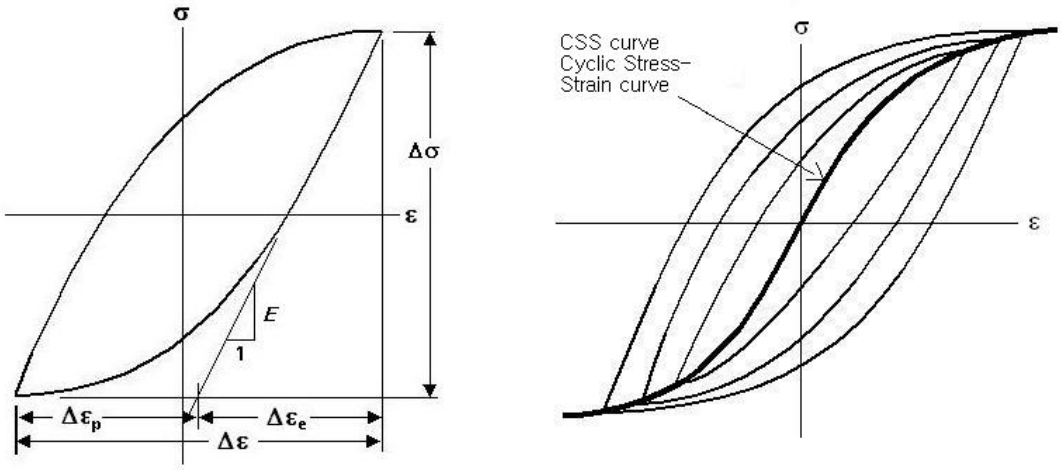

(a) Hysteresis curve (b) CSS curve

Figure 2.4: Cyclic deformation: (a) Hysteresis curve, (b) Cyclic stress-strain curve.

in the axial strain amplitude. Conversely, under constant-amplitude strain-controlled fatigue loading, an increase or decrease in the axial stress amplitude are caused respectively by hardening or softening of the material [7].

Attending to the manner of the variation of the hysteresis loops during the transient period, materials can be classified into three major categories. Materials presenting cyclic hardening or softening compose the two first groups. The third one consists of materials exhibiting both tendencies: initial cyclic hardening is followed by cyclic softening which ends after a certain number of cycles, when the saturation level is reached.

The transient period is caused by a continual change in dislocation substructure which eventually reaches a stable configuration representative of the saturated state. Beyond this point, in both cases, the respective strain amplitude and stress amplitude reach a stable saturation value. This saturation stage gives rise to stable hysteresis loops. The locus of the tips of stable hysteresis curves

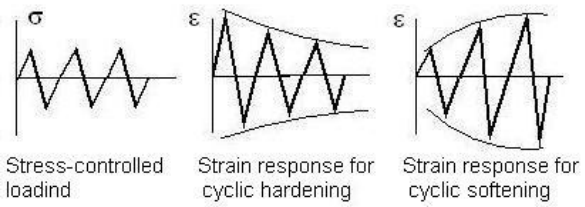

(a) Stress controlled loading

(b) Strain controlled loading

Figure 2.5: Transient phenomena: Hardening/Softening under (a)stress or (b)strain controlled loading.

provides the cyclic stress-strain curve, Figure 2.4(b).

Manson [14] proposes the most intuitive method for generating CSS curves. A series of samples are tested at several strain levels until the hysteresis loops stabilized. The stable hysteresis loops are then superimposed and the tips of the loops are connected by a line. This method is time consuming and requires many specimens. When only a few samples are available, an alternative procedure known as Incremental Step Test, may offer better results [15].

The Incremental Step Test method has become widely accepted, as it is very quick and provides good results. One specimen is subjected to a series of blocks of gradually increasing and decreasing strain amplitude. After a few blocks the material stabilizes. The cyclic stress-strain curve can be determined by connecting the tips of the stabilized hysteresis loops. After the Incremental Step

test, if the specimen is pulled to failure, the resulting stress-strain curve will be nearly identical to that obtained from Manson's method.

2.2.3. Crack initiation and propagation

Failure of a material due to fatigue may be viewed on a microscopic level in three steps:

- *Crack Initiation:* The crack initiates in this stage, also referred to as *Stage I*, which is the most time requiring part of the whole process.
- *Crack Propagation:* The crack continues to grow as a result of continuously applied stresses.
- *Failure:* It occurs when the material that has not been affected by the crack cannot withstand the applied stress and brakes very quickly.

The initiation of a crack is in great detail explained by some authors like [2] or [8]. The fatigue process is thought to begin at an internal or surface flaw which acts as a stress concentrator. After a large number of cycles, dislocations pile up and form structures called persistent slip bands (PSB). PSBs are areas that rise above (extrusion) or fall below (intrusion) the surface of the component due to movement of material or shear flow along slip planes. This leaves tiny steps in the surface that can serve as stress risers where fatigue cracks can initiate. One real crack running inward from an intrusion region may propagate along one of the original slip planes but eventually turns to propagate transversely to the principal normal stress as seen in Figure 2.6(b).

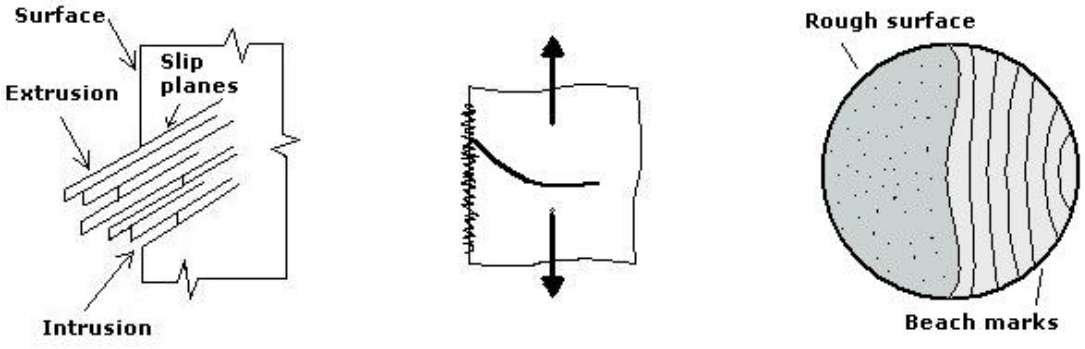

(a) Intrusions-Extrusions (b) Crack propagation (c) Crack Surface

Figure 2.6: Initiation, propagation and failure of a fatigue crack. (a) Dislocations piled up after a large number of cycles forming intrusions and extrusions. (b) Crack propagation transversely to the principal normal stress. (c) Clamshell and beach marks characteristic of a fatigued specimen

One can easily determine that a material failed by fatigue by examining the fracture surface, Figure 2.6(c). When the failure surface of a fatigued specimen is examined, a region of slow crack growth is usually evident in the form of a "clamshell" concentric around the location of the initial flaw. The clamshell region often contains concentric "beach marks" at which the crack was arrested for some number of cycles before resuming its growth. Each beach mark may contain thousands of "striations". Striations are thought to be steps in crack propagation, where the distance between them depends on the stress range. Striations are thought to be the advancement of a crack due to one cycle of loading. This region is smooth or brushed as a result of the rubbing of the bottom and top of the crack.

Eventually, the crack may become large enough to satisfy the energy or stress intensity criteria for rapid propagation. This final phase produces the rough or granular surface, typical of fast fracture.

2.2.4. Cumulative damage laws

The Palmgren-Miner hypothesis for damage accumulation, equation 2.6, postulates that a cycle of amplitude S_k consumes a fraction $1/N_{S_k}$ of the total life. Failure is predicted when the damage D exceeds 1 [3]. The law is described as,

$$D = \sum_k \frac{n_k}{N_{S_k}}, \tag{2.6}$$

where n_k is the number of cycles of amplitude S_k and N_{S_k} the number of cycles to failure, if only the stress amplitude S_k is applied.

According to [4], experiments point out that the summation on the right term of the equation, the damage D, is usually different from unity. Therefore, Palmgren-Miner relation should be considered as a guideline instead of a fixed design rule.

This is the simplest method available for fatigue life predictions. The simplicity is unfortunately accompanied by some weaknesses. Suresh points out one of them. The weakness he refers to is related to cyclic hardening or softening, which leads to different levels of stress relaxation during continued fatigue straining [7]. It is also well known the systematic error when using this rule together with a Wöhler curve based on tests at constant amplitude [3]. Likewise, sequence of loading is not taken into account [4] and can significantly affect the lifetime of a specimen. These are, among others, some drawbacks to be solved.

3. Experimental setting

3.1. 253MA

The material to be used in this thesis had already been chosen in the previous work. The selection procedure might be found in Borg's report [5].

The designation 253MA, commonly used in the literature, is not a denomination recognized by ASTM but a registered trade mark. Outokumpu [9] and other manufacturers like Atlas Steel Australia [10] provide different names for the grade which are listed below next to the chemical composition of the grade [11].

Outokumpu steel name	UNS No	Euronorm		Swedish SS
		Name	No	
32 253MA	S30815	X9CrNiSiCe21-11-2	1.4835	2368

	C	Ce	Cr	Mn	Ni	N	P	Si	S
min	0.05	0.03	20	-	10	0.14	-	1.4	-
max	0.1	0.08	22	0.8	12	0.2	0.04	2	0.03

Metal suppliers Online Inc. [11] as well as the steel manufacturer Atlas Steels Australia [12] describe this alloy as an austenitic stainless steel which combines oxidation resistance up to 1150 ℃ with high strength, good corrosion resistance and ease of fabrication. Applications include components requiring high strength at elevated temperatures such as radiant heating tubes, heat exchangers, heat treating oven components and kilns among others.

A complete compendium of mechanical properties of 253MA is available at the American manufacturer Haynes International Inc. web site [13], being the most outstanding features compiled in Table 3.1.

Temperature ℃	Elasticity Modulus [GPa]	Ultimate Tensile Strength [MPa]	Tensile Elongation [%]	0.2% Yield Strength [MPa]
21	200	717	51	350
700	145	445	44	166

Table 3.1: Mechanical properties of 253MA.

3.2. Standard Practice

In order to get reliable results, the experiments were performed according to the Standard Practice for Strain-Controlled Fatigue Testing [16], E606–92 (Reapproved 1998). This standard is under the jurisdiction of ASTM committee E-8 on Fatigue and Fracture and is the direct responsibility of Subcommittee E08.05 on Cyclic Deformation and Fatigue Crack Formation.

This practice covers the determination of fatigue properties of nominally homogeneous materials by the use of uniaxially loaded test specimens. It is applicable to temperatures and strain rates for which the magnitudes of time-dependent inelastic strains are on the same order or less than the magnitudes of time-independent inelastic strains.

All the procedures followed in this thesis observed the standard and the equipment fulfilled all the recommendations.

3.3. Sample design

The design of the samples had already been developed according to E606–92 for the previous thesis [5]. A sketch of the final design is shown in Figure 3.1 as well as a picture of a manufactured sample.

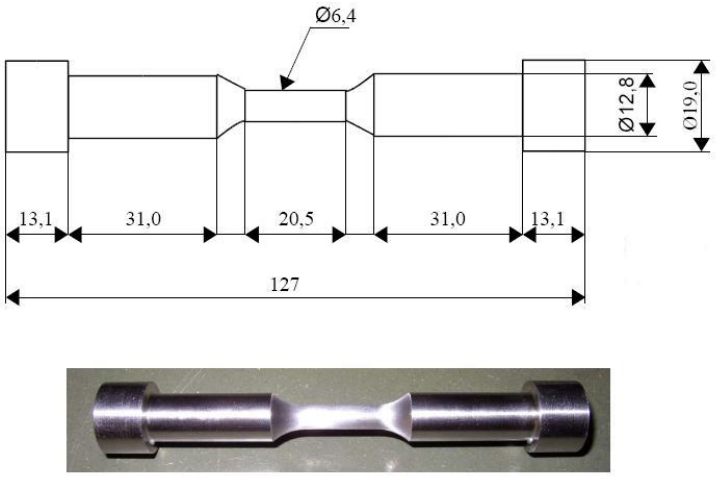

Figure 3.1: Sketch of the sample above and picture of a finished sample below taken from [5].

3.4. Equipment

The equipment necessary to perform the experiments was available at the laboratory. A testing machine, an extensometer and a furnace were the main instruments needed for the operation. Figure 3.2 shows an overview of the emplacement.

All the equipment to be used in the tests had to be adjusted prior to the experiments. The testing machine, the furnace and the extensometer were

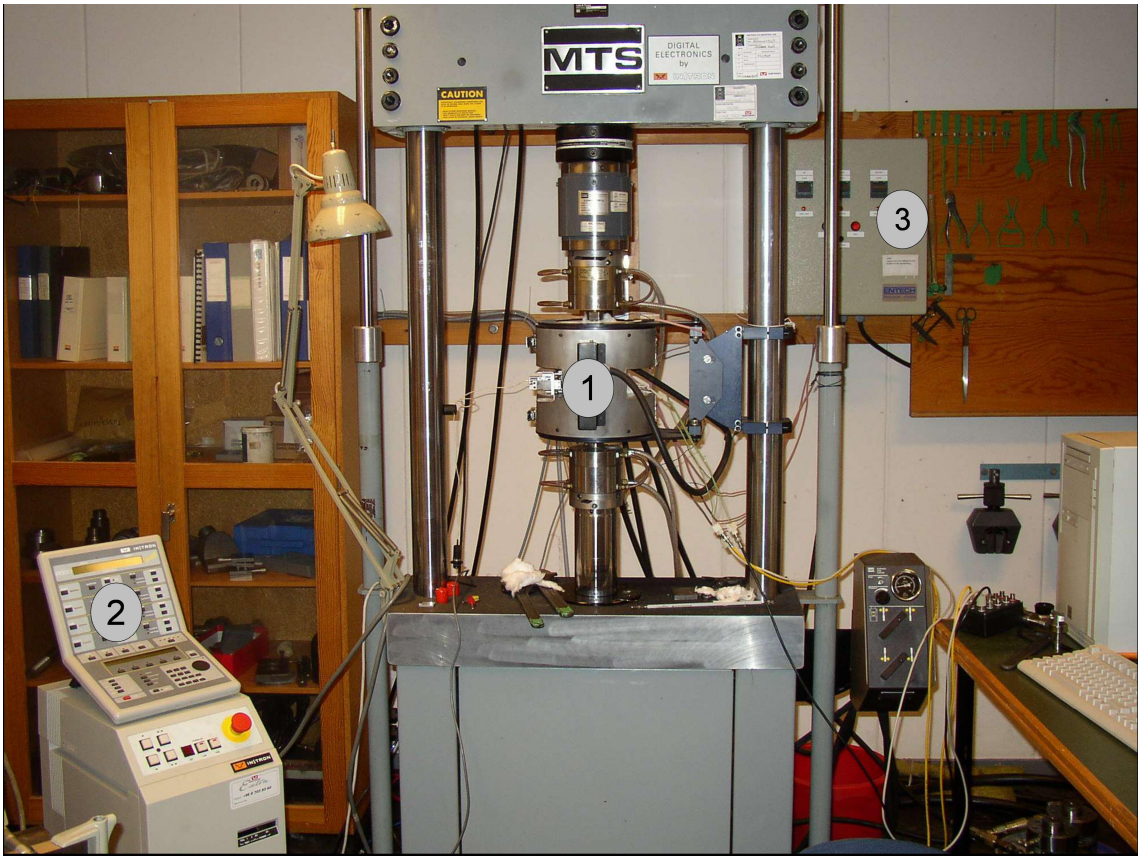

Figure 3.2: Overview of the emplacement and Testing Machine: furnace (1), Tower Console and Front Panel (2) and furnace control panel (3).

subjected to calibration to ensure a proper operation.

3.4.1. Testing machine

The testing machine Instron model 8500 Plus Dynamic Testing System consisted of a Tower Console and Front Panel, together with a load frame and actuator, a hydraulic power supply and a load cell as a load measurement device. These were all interconnected with electrical cables at the rear panel of the Tower Console [17]. The machine controls allowed cycling between constant strain

limits within the proper accuracy.

The Front Panel permitted an easy manipulation of the testing machine. The unit was prepared to perform several situations, including the few needed for these experiments. All the tests implemented at constant amplitude load were controlled by this panel.

At the same time, a computer was connected to the Tower Console. The experiments could then be controlled either through the Front Panel or through the data processor. Instron WaveMaker Software [18], available in this computer, was used to control the variable amplitude tests. This software provided an intuitive method to program the different blocks of a cumulative damage test.

A second computer was connected to the machine to log the output data. The applied force and the strain were stored in this way for a later analysis. The two analogue signals from the control unit were transformed into digital data by a signal converter installed in the computer. A manually started program written in LabVIEW [19] handled the data and created a three columns file containing the time referred to the computer's clock speed, the force and the strain.

The data were temporarily stored in the computer's working memory and saved only when the logging was stopped. As the working memory was very limited, the logging had to be stopped momentarily every hour to enable the software to write down the data in the file and liberate the working memory.

Fixtures. Alignment. The fixtures used to install the samples in the machine were the available ones in the laboratory. They were equipped with hydraulic tightening grips so to allow both negative and positive load. As they were to be

used at high temperature, a cooling system was required for each fixture. The cooling liquid was ordinary water.

In order to guarantee pure tensile tension, specimen fixtures were aligned such that the major axis of the specimen closely coincided with the load axis throughout each cycle. The standard E606–92 remarked the importance of a correct alignment and gave the necessary recommendations for a proper implementation [16].

In order to get such alignment, a specially prepared sample made of hardened steel and fitted with six strain gages was employed. The gages, stuck in pairs on the surface with 90° offset, were placed in the middle, lower and upper parts of the specimen.

Reading the output of the gages connected to an amplifier, the fixtures were adjusted to eliminate the bending and the transverse stresses.

It was not possible to eradicate all undesired stresses as the piston did not move exactly in the same way from cycle to cycle. Nevertheless, the order of magnitude of these strains was low enough to justify the neglect of the remaining secondary stresses.

Furthermore, it was concluded that there was no need for further adjustments every time a new sample was installed in the machine, as the already acquired precision lay within the limits prescribed by the testing standard [16].

3.4.2. Furnace

A furnace was indispensable as the tests were to be performed at 700 ℃. A vertical tube furnace, model ESTF 60/11-III manufactured by Entech, suitable for material testing was already mounted onto the testing machine [20].

The ESTF-type was a high temperature furnace with features especially suited for tension/compression fatigue testing of metals. The heated length represented more than 85% of the total height and consisted of three individually operated zones, powered by three 600 W thermal elements. The three zone control of this furnace resulted in very good temperature control over a large part of the total heated length. The elements were embedded in ceramics fibre in six half shells, which were independently exchangeable.

The controllers used digital PDSIO master-slave communication, being the central one the master, and the other two the slaves. Once the temperature was selected in the master control, the others just adopted the set value.

Three thermocouples indicated the actual temperature of the different parts of the heated length to the control unit which adjusted the corresponding supplied power in order to reach and maintain the desired temperature homogeneously along the specimen.

The split design allowed an easy installation and removal of the samples as the furnace could be opened by pulling apart the two halves. However, this design in combination with the fact that the machine was continuously moving up and down generated some leaks, as it could not be hermetically closed. Mineral wool was placed in the possible ways out to reduce the leakages.

Furnace calibration. A calibration of the furnace was implemented to ensure the proper operation of the device. Three thermocouples were micro welded onto one sample installed in the testing machine. The thermocouples were equally separated over the surface, covering the whole length of interest of the sample. Then the furnace was closed and the temperature set to 700 ℃.

After some hours, the furnace indicators displayed 700 ℃ in the three units. In spite of this, the thermocouples pointed that the temperature at the surface of the sample was not homogeneous. 705 ℃, 698 ℃ and 702 ℃ respectively, were the registered values indeed.

The starting offset values of the controllers were the ones obtained by Borg [5] being touched up until a better result was obtained. At that point, the temperatures appointed by the thermocouples were 700 ℃, 702 ℃ and 695 ℃ with offsets of -51, -43 and -68 respectively.

To further verify the calibration, the thermal expansion of the metal was measured in some samples. A value of 1.2% was observed in most of the samples, matching the data given by the manufactures (Table 3.1). This indicated that the temperature reached by the specimens was 700 ℃ as desired.

3.4.3. Extensometer

A high temperature axial extensometer, model MTS 632.53/54 was used to measure the strain of the samples. As the product manual [21] pointed out, the extensometer used precision ground ceramic extension rods to extend into the hot zone of the furnace. With the extension rod ends contacting the specimen, the instrument was held in position by a spring-loaded hold-down assembly attached

to the furnace. A low specimen contact force per extension rod minimized the possibility of damage to the specimen which could cause premature failure.

Air cooling was necessary as the temperature was above 650 ℃. The cooling system was attached to the furnace pointing to the extensometer as can be appreciated in Figure 3.3.

A calibration was performed prior to testing. A 20% strain range was gauged by means of a micrometer screw. Young's modulus of a random sample was measured to ratify the calibration process undergone.

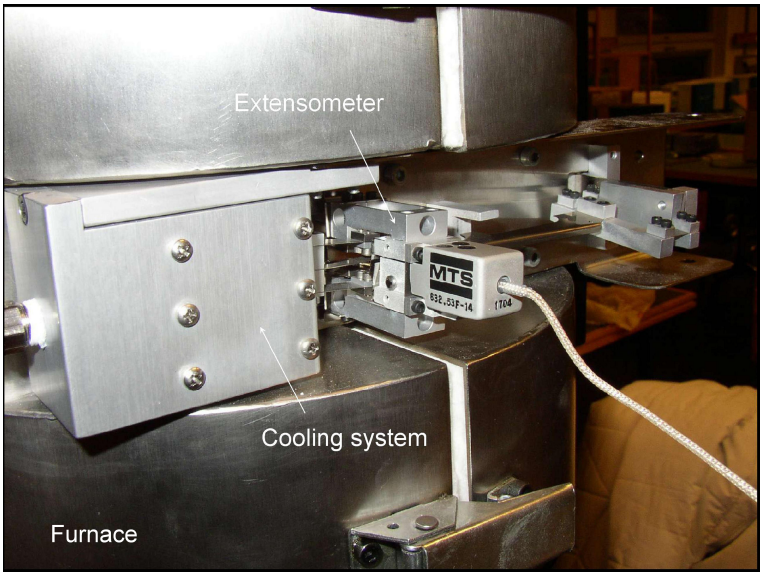

Figure 3.3: Extensometer and cooling system attached to the furnace.

3.5. Experiments

Once the equipment was arranged, a test plan was designed and the experiments implemented.

3.5.1. Test plan

A first planning including just a few samples was set, waiting for some results to decide which conditions were more relevant to be tested in the remaining samples.

The tests to be performed were mostly under variable amplitude fatigue conditions. In these tests, the strain amplitude varied alternately between two fixed values, defining so, two different loading blocks.

A temperature of 700 ℃, frequency of 0.5 Hz and ratio R of -1 were set the same for all experiments, differing from one another solely in the strain range values.

The strain values were selected to be comprised within the studied range in Borg's thesis [5], that is from 0.5 to 0.8%. Notwithstanding the schedule, the first samples were performed at higher load levels by mistake. The new data points, which lay out of the investigated range, did not fit the expected endurance.

It is well known that classical methods of calculating fatigue life from S-N curves provide acceptable results when the stress level is not high. In these cases, lives of elevated number of cycles are produced ($10^5 \div 10^6$) and the deformations are essentially elastic. Most of the lifetime is consumed in crack nucleation, while propagation occurs in a short time interval. Fatigue is considered to be one whole process until failure.

However, at high stress levels, considerable plastic deformations appear, producing the nucleation after just a few cycles. Most of the time is employed on propagation. In these cases, Fracture Mechanics techniques are applied to the study of the failure process, separating nucleation and propagation into two

different periods. S-N curves give way to ε-N ones, relating the deformation to the number of cycles to crack initiation.

The common practice of using different methods in fatigue life predictions depending on the stress level does not justify enormous differences when using either one of these approaches to the same range. For this reason, the unexpected results obtained at high stress level could have brought into the open a possible change of behaviour at this level of load. It was considered interesting and the test plan was adapted to cover this higher range of amplitudes. The final version of the test plan is presented in Table 3.2.

As can be seen in Table 3.2, samples 1, 2, 15 and 16 were subjected to constant amplitude loading. The two former were aimed to check whether the results obtained were comparable to the available data provided by Borg [5] or not. The two latter were necessary to acquire data from high load levels, as it had been observed a different behaviour under high loading.

The rest of the samples were subjected to variable amplitude testing. Albeit cumulative fatigue damage was the main topic of this research, some particular combinations of testing conditions wanted to be investigated at the same time. Researches in the field pointed out that the sequence of loading could significantly affect the lifetime [4]. Thus the block order of samples 3, 5 and 8 was switched resulting samples 4, 6 and 9.

Samples 10, 11 and 13 differed just in the length of the second block to investigate whether the ratio of number of cycles of both blocks had an influence in the results.

Finally, tests number 10, 12 and 14 were performed at the same strain ranges to

	First block		Second block	
Sample	$\Delta\varepsilon$ [%]	N_{B1}	$\Delta\varepsilon$ [%]	N_{B2}
1	0.55	-	-	-
2	0.80	-	-	-
3	1.00	500	1.60	100
4	1.60	100	1.00	500
5	1.30	100	1.60	1
6	1.60	1	1.30	100
7	1.00	100	1.60	10
8	1.00	100	1.60	50
9	1.60	50	1.00	100
10	0.50	100	0.80	100
11	0.50	100	0.80	10
12	0.50	100	0.80	100
13	0.50	100	0.80	1
14	0.50	100	0.80	100
15	1.60	-	-	-
16	1.00	-	-	-

Table 3.2: Strain Controlled Fatigue Test Plan.($N_{B1,2}$:Number of cycles of the first and second block)

check the repeatability of the experiments.

3.5.2. Test performance

The test plan in Table 3.2 was carried out without any further modification. No major incidents interfered with the process.

The slip of the extensometer rods was a problem in previous works using the same equipment. As recommended from experience [5], a compression load of 3 kN was applied during the heating process. In this way, the hydraulic system stayed working avoiding vibrations at the starting which could cause the slip of the rods. Right before the tests were run, the compression load was released and a tiny tension load was applied, forcing the pistons into a smooth movement. Thanks to this procedure, the slip of the rods was avoided.

The signal feed was sent through a coaxial cable from the Tower Console to the logging computer. External noise could not be avoided. During the last experiments, the static testing machine situated next to the computer was being used interfering with the signal. Nevertheless, it did not hinter the research.

4. Results

Once the tests were implemented, the results were compiled and analyzed. The most relevant outcomes are explained in this section.

Files containing the force and deformation applied to each specimen and the number of cycles to failure, were the only data directly obtained from the experiments. However, after some calculations, other indirect results were computed. The Young's modulus, the stress and the plastic and elastic strains undergone by the samples were found in this way. These data were employed with two different objectives: the validation of the experimental data and the development of a mathematical model for the behaviour of the material under variable amplitude loading conditions.

The most outstanding results are gathered in Table 4.1.

4.1. Validation of the data

As already mentioned, a previous paper on constant amplitude fatigue at high temperature had been written by Borg [5]. As the material and the conditions were the same in both cases, it was interesting to gather the data and the calculations already performed so they could be used as a basis for this thesis. In order to check whether the new data collected in this project were consistent with the literature and with Borg's calculations, some comparisons were carried out.

The first step was to compare the elastic modulus, E, also known as *Young's modulus* [22]. This modulus of elasticity was a measure of the stiffness of a given

Sample	$\Delta\epsilon_{p1}$	$\Delta\epsilon_{p2}$	N_f
3	0.606	1.183	1277
4	1.109	0.577	695
5	0.835	1.117	808
6	1.193	0.871	708
7	0.598	1.104	1210
8	0.570	1.150	1050
9	1.131	0.566	800
10	0.143	0.406	3616
11	0.161	0.448	5551
12	0.143	0.414	3578
13	0.161	0.453	10425
14	0.141	0.407	2729

Table 4.1: Most outstanding results from the experiments. ($\Delta\epsilon_{p1,2}$: plastic strain range, blocks 1, 2; N_f: cycles to failure)

material and thus had to be the same for all the samples tested in both thesis works. This value also had to be the same as the ones provided by the manufactures.

In order to minimize differences and provide a reliable comparison, the method employed to determine Young's modulus was the same as used in the previous thesis. Both the force and the strain undergone by the samples were logged during the experiments so that it was possible to determine the stresses. Once collected both strains and stresses, the hysteresis curves were drawn for every sample and the Modulus measured from them with the support of software written in MatLab [23].

Figure 4.1 shows the hysteresis curves of one of the samples created from the measured data. It can be observed that the plot was very similar to the theoretical one, presented in Figure 2.4(a) in section 2.2.2. According to [22], the slope of the stress-strain curve represented Young's modulus. As the author stated, the modulus was the initial, linear elastic slope of the curve. Following the recommendations, the modulus was measured at the straight part of the curve at beginning of the loop, where the material was solely elastically deformed.

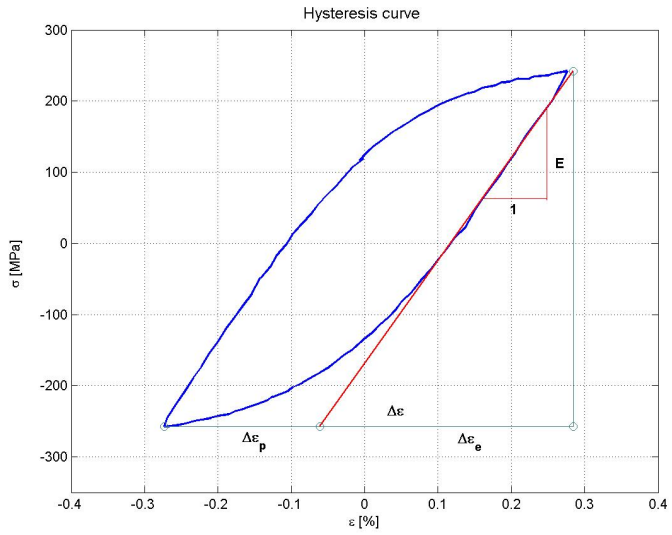

Figure 4.1: Hysteresis curve obtained from the experimental data. E, $\Delta\epsilon$, $\Delta\epsilon_e$ and $\Delta\epsilon_p$ can be calculated from the plot.

The modulus was estimated in this way for all the samples obtaining a set of pretty uniform values with a mean value of 141 GPa and a standard deviation of 4 GPa (2.5%). These numbers fitted well with Borg's results [5] who had provided a mean value of 142 GPa. Furthermore, the manufacturer Haynes [13] claimed an elastic modulus of 145 GPa for this alloy (See Table 3.1). The difference between all these values was negligible, concluding that the experiments were correctly implemented and the data trustworthy.

A complementary validation was carried out by the execution of some tests under

constant amplitude loading. As Borg's results could predict the lifetime of a sample under constant amplitude loading, it was interesting to check his predictions, testing an extra sample. In this way, sample number 2, in Table 3.2, was subjected to constant amplitude load testing. The conditions were selected within the studied range of amplitudes. The test provided an endurance very similar to the prediction, indicating no anomalies in the processes. The outcome of this test is shown in the following tabular along with the the prediction of life by Borg's approach.

Sample	Predicted N_f	Actual N_f
2	1636	1745

A third and last comparison proved the reliability of the experimental work: The plastic strains of the samples were estimated by two methods and compared later on. The former based on Borg's results while the latter used the new experimental data.

The first method was based on the conversion plot calculated by Borg [5], Figure 4.4. This plot provided the plastic strain directly from the total strain thus it was immediate to get the values. The meaning and the utility of this graph will be later explained into detail in section 4.3.1.

In the other way of calculation, the hysteresis curves obtained from the experimental data was the only source of information. The plastic and elastic strains could be found from the hysteresis curve easily. As seen in Figures 2.4(a) and 4.1, the same line drawn to determine Young's modulus might be used to identify both plastic and elastic strains. The width of the loop represented the total strain range and was divided by the auxiliary line into plastic and elastic strain ranges.

Table 4.2 presents both sets of plastic strains achieved by these two methods did not importantly differ, standing out the goodness of Borg's conversion plot and justifying its next use.

	Plastic Strain		
Sample	Hysteresis curve	Conversion plot	Difference [%]
3	0.606	0.574	5.612
4	0.577	0.574	0.558
5	0.835	0.824	1.323
6	0.871	0.824	5.691
7	1.104	1.074	2.755
8	0.570	0.574	-0.662
9	0.566	0.574	-1.359
10	0.406	0.407	-0.221
11	0.161	0.157	2.810
12	0.414	0.407	1.745
13	0.161	0.157	2.810
14	0.407	0.407	0.025

Table 4.2: Plastic strain ranges obtained from the hysteresis curve (experimental data) and from the conversion plot (Borg's data [5]).

All these comparisons leaded to a clear conclusion: The experimental work was reliable and the data trustworthy. The data and results from Borg's thesis could be used as a basis for this one.

4.2. Analysis of the data

4.2.1. Cyclic Stress Strain Curve

Once the data were validated, the cyclic stress-strain curve of the material was obtained. As expounded in section 2.2.2, when a material was subjected to cyclic load, the stress and the strain defined hysteresis loops. The locus of the tips of these hysteresis curves delineated the cyclic stress-strain curve, CSS, Figure 2.4(b).

Manson's method and the Incremental Step Test, described in section 2.2.2, were the most outstanding procedures for generating a CSS. In this thesis, neither one of the explained methods was employed. Indeed, the idea of both tests were blended into the one used here though. Several samples had been already tested. Some of the trials had been performed under constant amplitude loading although most of them had been subjected to two different blocks of strain amplitude. Therefore, considering that the loops reached the stability in every block, at least one point of the desired plot could be extracted from each test.

The CSS curve obtained from the application of the exposed methodology is presented in Figure 4.2. In order to plot the monotonic stress-strain curve on the same graph to emphasize the difference between both curves, the first cycle of one of the samples has been extracted and plotted along with the CSS curve points. One can notice that the CSS curve lay above the monotonic one due to cyclic work hardening.

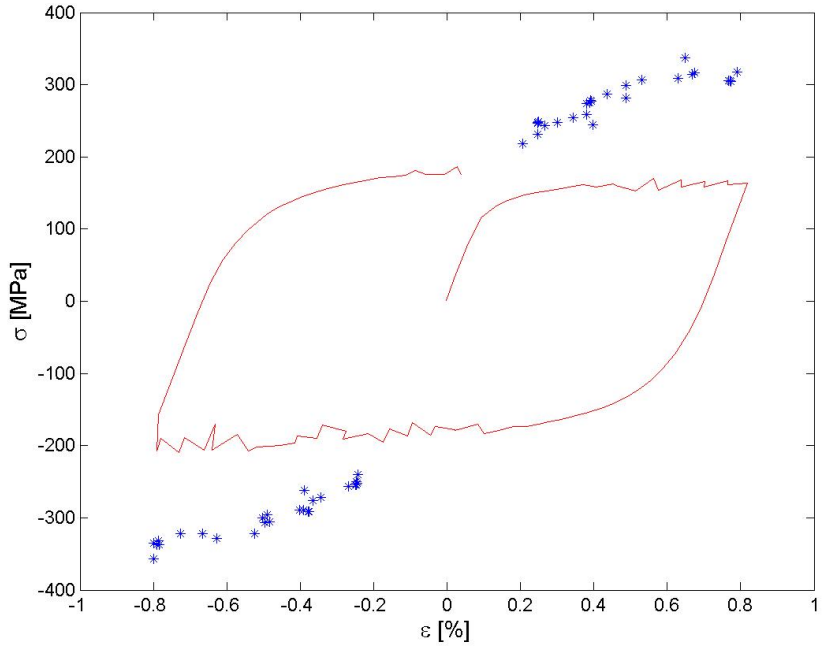

Figure 4.2: Cyclic Stress-Strain curve along with monotonic stress-strain curve for 253MA.

4.2.2. Cyclic work hardening /softening

Low cycle fatigue was dominated by the plastic strain [6]. Therefore, it was attractive to deeply analyze this physical magnitude in order to understand the behaviour of the material under variable load amplitude.

As mentioned in section 2.2.2, there was a correlation between the stress and the strain under cyclic load conditions, defined by the cyclic stress-strain curve, CSS, Figure 2.4(b). Thus, one could expect the same level of stress and plastic strain at a certain deformation range. However, this curve represented a steady-state situation and did not describe any transient phenomena effects. When the strain range was varied, there was a short period in which the tips of the loops did not lie on the curve. The tips described a different path non-coincident with the cyclic stress-strain curve, reaching the steady state after up to 100 cycles or half

lifetime in most cases. Those paths corresponded either to work hardening or softening of the material [7].

As the tests were run under variable amplitude loading, the transient period became noteworthy. Whether the samples were subjected to work hardening or softening could be a hint of the fatigue lifetime. In the case of softening, the sample underwent higher stresses than the corresponding to the steady state, thus, longer life could be expected as lower plastic strain ranges were applied.[1] Conversely, shorter lives could be expected to be produced by work hardening.

All the samples presented a complex combination of both phenomena along the whole curve. A initial hardening stood out in every test, in all cases accompanied by a continuous slow softening all over the duration of the experiment. In addition, a strong hardening arose after every load increase, as well as a strong softening appeared when the load decreased. Interestingly, samples undergoing constant amplitude load did not show this features [5]. Figure 4.3 exemplifies this complicated composition.

It can be perceived in the graph that the hardening that appeared at the changing of the blocks was of the same magnitude than the strong softening afterwords. Both effects seemed to be balanced. On the other hand, despite the continuous stress level decrease, the CSS curve lay above the monotonic one, since the initial hardening was much stronger.

[1] Higher stress ranges lead to lower plastic strain ranges at a certain strain range.

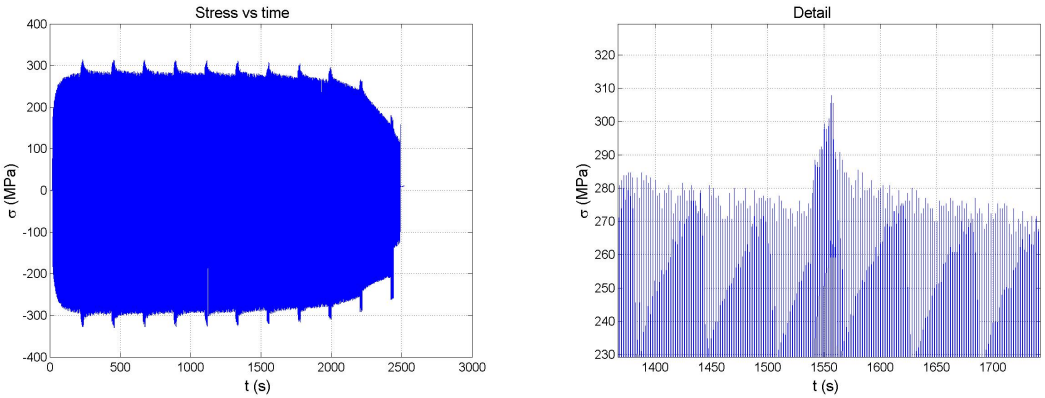

(a) Sample 7

(b) Detail of a peak

Figure 4.3: Transient phenomena. Cyclic work Hardening / Softening

4.3. Predictions of fatigue life. Palmgren-Miner law

One of the main objectives of this thesis was to analyze the reliability of Palmgren-Miner law, equation 2.6, which gave an estimation of fatigue life under variable amplitude conditions. In order to achieve this goal, the predicted fatigue lives given by this law were compared to the actual fatigue lives collected from the experiments.

However, as explained in section 2.2.4, it was necessary to know the number of cycles to failure at constant amplitude for predicting the fatigue life of elements under variable amplitude loading. Hence, a constant amplitude strain-based curve was developed.

This curve provided the number of cycles to failure at constant amplitude versus the plastic strain range undergone by the sample. Thus, in order to apply the desired equation 2.6, one needed to obtain the plastic strain range in the first place. After that, the number of cycles to failure could be found using the

constant amplitude curve, so that it was possible to finally apply Palmgren-Miner law. The general procedure is summarized in the following diagram:

Plastic strain range	⇒	Number of cycles to failure at constant amplitude	⇒	Predictions by Palmgren-Miner law

4.3.1. Plastic strain range. Conversion plot

As commented at the beginning of this subsection, the first step in the prediction of cumulative fatigue life was based on the plastic strain which was unknown prior to testing. However, testing was not always possible when designing a new element. Therefore, a method to calculate the plastic strain from the data available prior to testing had to be developed if these methods were to be applied in future designs.

This problem could be overcome utilizing a conversion plot, which related the total strain range to the plastic one. A curve of these features had been previously developed for 253MA by Borg [5]. It was calculated as a regression line through the experimental data. The use of this plot, sketched in Figure 4.4, has been previously justified in Section 4.1.

One last consideration concerning this curve was the fact that it was a steady state curve employed in a variable amplitude experiment where the steady state might not be reached. Considering cyclic work hardening and softening as the only influential transient phenomena, the analysis was easily carried out. When a sample was subjected to cyclic work hardening, the plastic strain ranges undergone were higher than the steady state ones. Conversely, the plastic strains

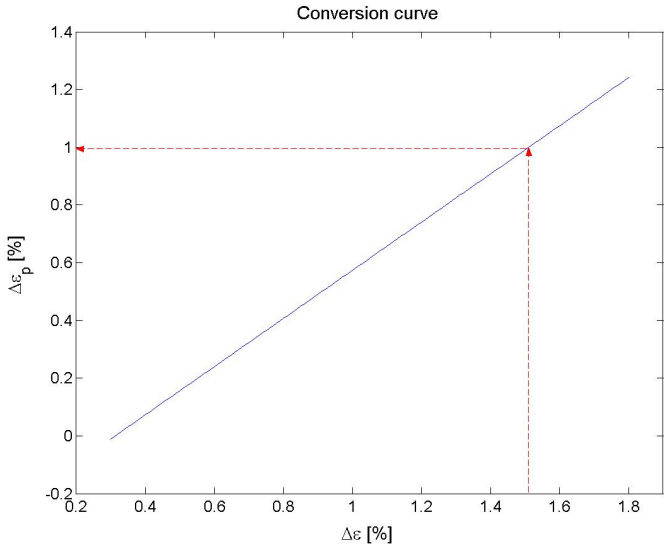

Figure 4.4: Plastic strain vs. strain range

were smaller when softening occurred. However, the effects of these transient phenomena, as already analyzed in the previous section 4.1, seemed to be self-balanced. As the sample was subjected to both hardening and softening, the conversion plot could be understood as the mean value of the plastic strains. The interpretation of the initial strong hardening and the continuous slow softening, which was the major weakness of Palmgren-Miner law, was still a problem to be solved.

4.3.2. Constant amplitude curve. Coffin-Manson relationship

The next step for the predictions of lifetime was obtaining a constant amplitude curve. Nevertheless, it was not necessary since it had been already developed in the previous thesis [5]. This curve was a strain-based approach to total life based on the Coffin-Manson relationship, equation 2.2, which could also be expressed as equation 4.1.

$$\ln(\Delta\varepsilon_p) = -\beta \cdot \ln(N) + \ln(C_2) \tag{4.1}$$

The values of the material constants (β and C_2) were calculated from a least squares fitting curve of the experimental data, described by equation 4.2, valid for 253MA at 700 ℃.

$$\Delta\varepsilon_p \cdot N_f^{0.5566} = 0.2502 \tag{4.2}$$

This equation indicated a linear relationship between the plastic strain ($\Delta\varepsilon_p$) and the number of cycles to failure (N_f) under constant amplitude loading, as can be seen in Figure 4.5.

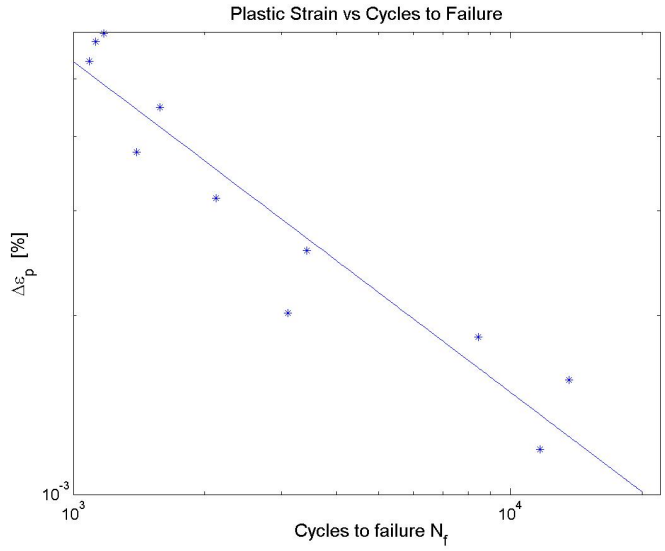

Figure 4.5: Coffin-Manson Relationship: plastic strain ($\Delta\varepsilon_p$) vs cycles to failure (N_f)

4.3.3. Predicted versus actual fatigue lives

The general procedure to predict the fatigue life under variable load amplitude started with the calculation of the plastic strain from the conversion plot, Figure 4.4. These values were used in Figure 4.5 to get the number of cycles to failure when constant strain amplitudes were applied.

Therefore, there was just one step left to achieve the objective. Considering that

failure occurred when the damage D in equation 2.6 exceeded 1, a prediction of life was achieved for every combination of strain amplitudes and number of cycles.

Table 4.3 presents the predictions along with the real duration of the tests.

Sample	N_p	N_r	N_r/N_p
3	674	1277	1.9
4	624	695	1.1
5	458	808	1.8
6	457	708	1.5
7	757	1210	1.6
8	557	1050	1.9
9	489	800	1.6
10	2785	3616	1.3
11	6451	5551	0.9
12	2785	3578	1.3
13	8703	10425	1.2
14	2785	2729	1.0

Table 4.3: Predicted (N_p) and actual (N_r) duration of the tests

The last column of the Table 4.3 contains the ratio of the real duration of the test to the predicted one. This ratio represented also the value of the summation $\sum_k \frac{n_k}{N_{S_k}}$ in the right term of equation 2.6. The values were close to unity for all the samples, within the common limits in any case (See section 2.2.4). A noteworthy fact was that besides one exception (sample 11), they were all conservative, specially at high load (samples 3 to 9).

In conclusion, it could be said that the prediction of fatigue lifetime by Palmgren-Miner law was rather satisfying.

4.4. Alternative constant amplitude curves

The appreciable difference between the accuracy of the predictions for high and low loads suggested a possible dependence of the material behaviour on the load level. In case this suspicion was correct, the constant amplitude curve defined by the Coffin-Manson relation, Figure 4.5, developed for low loads could be leading into error. In order to reveal whether the plot was valid for the entire range of interest or not, two samples were tested under high load conditions.

Samples 15 and 16, in Table 3.2, were thus tested at constant-amplitude high-load, confirming the suspicion experimentally. The new points did lie neither on nor close to the curve, proving the discordance between the model and the real behaviour. It seemed that the slope of the curve was too small at high level, producing considerable shorter lifetimes in this range of load. The results of these tests are gathered in the following tabular along with the predicted values.

Sample	Predicted N_f	Actual N_f
15	286	629
16	882	1350

The need of improvement of the constant amplitude curve induced the implementation of two alternative approaches, based the former on the total strain range and the latter on the plastic one.

4.4.1. Total strain range approach

Coffin-Manson relationship considered that the effect of the elastic strain was negligible in LCF. However, the different response at different load levels suggested that the elastic strain could play an important role in the failure of the material. Furthermore, the new points gathered from the additional tests indicated that the curve should be bended in order to fit them in. This curved shape resembled the total strain range approach curves.

Those observations aroused the idea of using the total strain range instead of the plastic one, so that the influence of the elastic strain, if any, would be enclosed.

Strain-range approach to total life, described by equation 2.3 in section 2.2.1 was thus employed in the new approach. The two terms on the right side of the equation represented the plastic and the elastic strain ranges respectively. The parameters of both fitting curves were calculated separately by MatLab curve fitting tool [23]. The resulting the expression, equation 4.3, is represented in Figure 4.6.

$$\frac{\Delta\epsilon}{2} = 0.005011(2N_f)^{-0.1149} + 0.379(2N_f)^{-0.6323} \tag{4.3}$$

The prediction process was carried out again, considering this time, this new constant amplitude plot. The satisfying outcomes are collected in Table 4.4.

The improvement of the results with the use of this new constant amplitude plot was notorious. The predictions, which were still generally conservative,

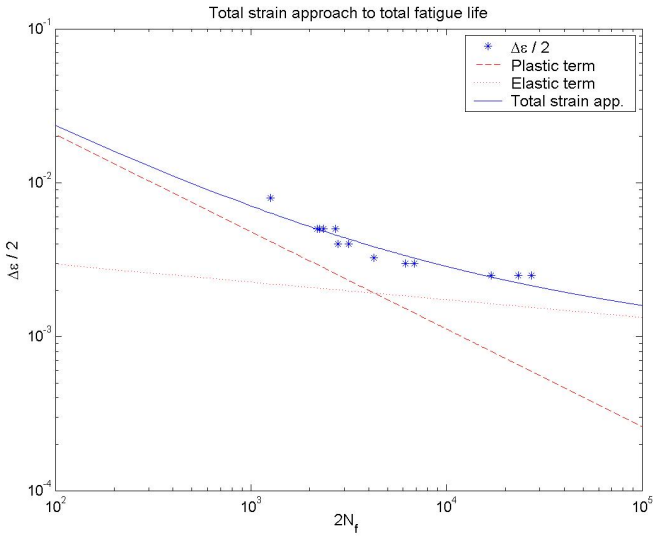

Figure 4.6: Fitting curve. The data set includes new samples 15 and 16.

approximated the real test durations with a higher accuracy, specially at high amplitude level (samples 3 to 9).

A deeper analysis explicates the reasons of the melioration. As commented above, a improvement was needed at high loading levels. However, at low loads, the performance of Coffin-Manson relation was satisfactory. The slope of the constant amplitude curve, Figure 4.2, seemed to be too small at high loads. The melioration was achieved applying this new curve which had a higher slope at those load levels. The former curve only contained the plastic strain, while in the new one, both plastic and elastic strains were enclosed. In addition, the plastic term in the second approach had a higher slope producing this melioration at high loads. At low loads, this increase of slope was balanced with the addition of the elastic term, which tended to decrease the slope. In conclusion, at low loads the predictions were not affected by using the new approach while at high loads an improvement was achieved.

Sample	N_r/N_p Original model	Total strain model	Combined plastic model
3	1.9	1.4	1.5
4	1.5	1.3	1.3
5	1.8	1.4	1.5
6	1.5	1.2	1.3
7	1.6	1.3	1.3
8	1.9	1.5	1.6
9	1.6	1.2	1.3
10	1.3	1.2	1.1
11	0.9	0.9	0.7
12	1.3	1.1	1.1
13	1.2	1.4	1.0

Table 4.4: Predicted (N_p) to actual (N_r) duration ratio of the tests for the different approaches.

The fact that a Total Strain approach fitted so well the data as well as the visual observation of the plot, led to the thought that the test conditions pertained to the transition between LCF and HCF. However, the lack of data from the whole range of the graph impeded the confirmation of such idea.

4.4.2. Combined plastic strain range

Theoretically, the samples were tested under low cycle fatigue conditions. The literature on this subject suggested that the elastic strain had negligible effect on the endurance. For that reason, a new approach which considered solely the

plastic strain range was implemented.

The purpose of this new curve was to improve the accuracy at high load level of the original constant amplitude curve, described by Coffin-Manson relationship. In order to reach this aim, the results obtained from samples 15 and 16 (constant amplitude tests), were included in the initial data set, found in [1]. Inspired in the previous method, equation 4.4 was proposed as an alternative method of fatigue lifetime prediction.

$$\frac{\Delta\epsilon_p}{2} = \frac{\sigma'_f}{E}(2N_f)^b + \epsilon'_f(2N_f)^c, \tag{4.4}$$

MatLab curve fitting tool [23] provided the values of the parameters of the proposed formula, resulting equation 4.5.

$$\frac{\Delta\epsilon_p}{2} = 0.1983(2N_f)^{-0.5526} + 9.459(2N_f)^{-4.866} \tag{4.5}$$

It was remarkable that the second term on the right side of equation 4.5 was negligible. Furthermore, this approximation did slightly differ from the original one as the slope of the curves was almost the same. Figure 4.7 shows how both lines almost overlapped. However, this approach surprisingly led to better predictions of lifetime although less conservative (see Table 4.4).

4.5. Particular cases

Some other interesting tips were deduced observing the performance of the samples under certain conditions (see Tables 3.2 and 4.4). The unequal responses of the samples had some common features, which might reveal some possible

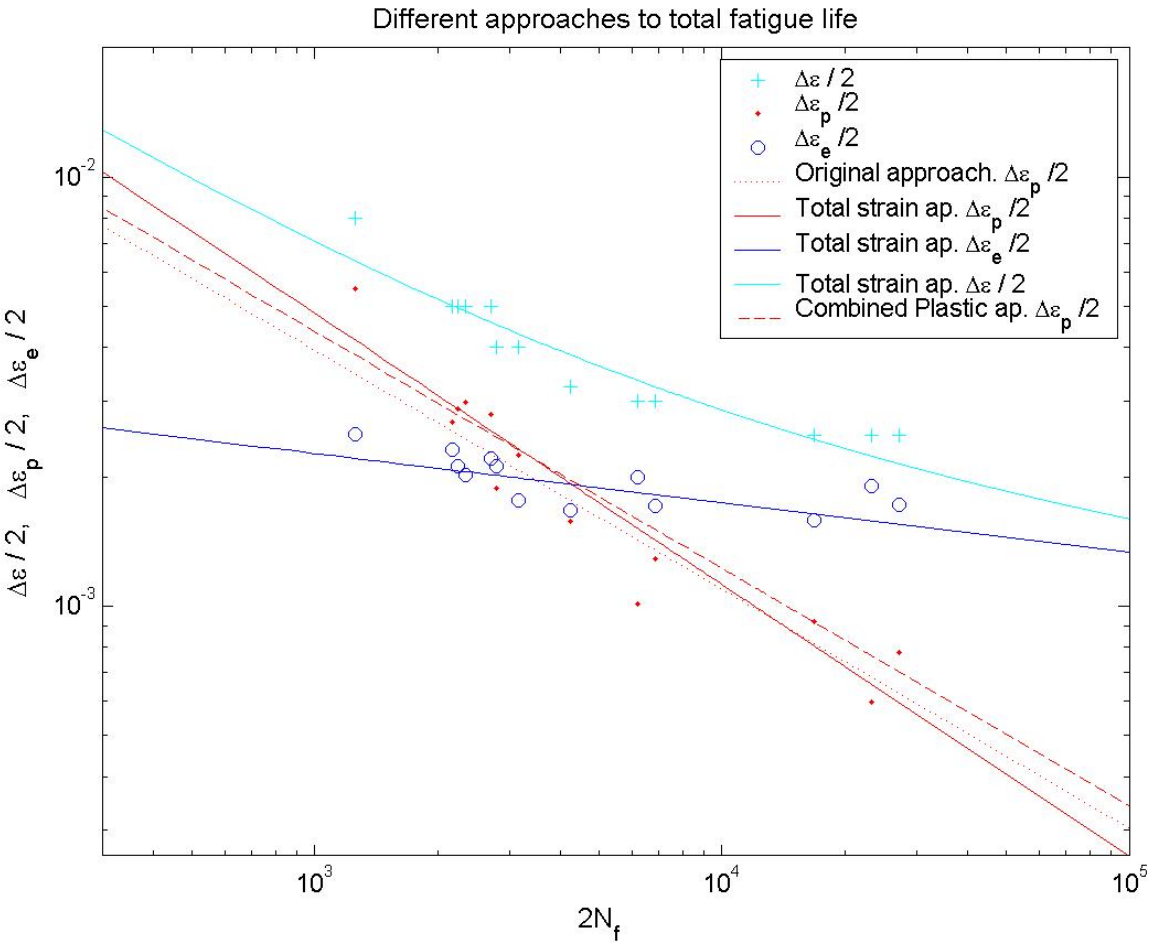

Figure 4.7: Different constant amplitude curves: It can observed that the original or Coffin-Manson approach nearly overlaps the last one, based on a combined plastic strain. The Total Strain approach composed of both elastic and plastic strains also fit properly with the data.

behaviour patterns under variable amplitude load. Two cases were worthy of consideration:

Case 1. Block timing variation. Samples undergoing blocks of the same load amplitudes, differing just in the duration of the second block, had not the same response. Pairs 7–8 and 10–13 symbolized

this combination of blocks with the same load amplitude but different duration at high load (see Table 3.2). The experiments apparently indicated that the shorter the second block, the more aggressive it was, resulting in a less conservative prediction of live.

Case 2. Sequence alteration. Samples undergoing the same blocks in switched order had an unequal reaction. Samples 3–4, 5–6 or 8–9 were examples of this case of symmetrical blocks: same load, different order. It seemed that the higher load was more harmful when applied in the first place. Some calculations were performed by software written in MatLab [23] to get the average of the maximum stresses of the experiments which could explain this peculiarities. No difference between the average stress level of the symmetrical tests was found. This fact pointed to the microscopic phenomena as the responsible for these unexpected responses.

The experimental results were consistent with the hypothesis of the existence of these behaviour patterns. Besides one exception, sample 11, which had an unexpected shorter life, the relative duration of the tests could be explained satisfactorily assuming this hypothesis to be true. Possible flaws in the specimen might be the reason of the early failure of sample 11. Nevertheless, more tests were needed in order to make a firm statement.

5. Conclusions

The main goal of this project was the startup and readjustment of the fatigue testing equipment, available at the division of Material Sciences at LTH. To reach this aim, high temperature low-cycle variable-amplitude fatigue testing on stainless steel grade 253MA was implemented in 16 samples. At the end of the project, the fatigue testing machine was ready to use.

The second aim was to research on the accuracy of Palmgren-Miner rule for cumulative damage predictions. Along the course of this study, the effects of three particular cases were analyzed: switched test sequence, prolonged relative duration of blocks and peak loads. The experimental data indicated that these particular situations affected the endurance of the material.

The data from the tests showed that such rule was a valuable method for a first conservative evaluation. It showed two major weakness though. The former was a strong dependence on the constant amplitude approach employed in the calculations; The latter was the lack of description of some effects such as sequence alteration.

This research also revealed that Coffin-Manson relationship could not describe properly the fatigue behaviour of the material under constant amplitude conditions. From the alternative approaches proposed, the Total Strain approach to fatigue life was the most accurate.

A future research in this field could be oriented to a obtain a complete model, capable of rationalizing effects such as the observed in this project. A first idea could be to enclose these particular cases into numerical factors so that the

condition of safety would be guaranteed.

Nevertheless, the major limitation of this investigation was the lack of data to make definitive conclusions. Obtaining data from a wider range of load amplitudes would allow the development of a better constant amplitude fatigue curve. This would confirming whether the hypothesis of LCF was correctly assumed.

References

[1] *Elevated-Temperature Crack Growth of Structural Alloys*, ASM Handbook Volume 19: Fatigue And Fracture, 1996.

[2] Roylance D., *Fatigue*, MA 02139, Department of Materials Science and Engineering, Massachusetts Institute of Technology, Cambridge, 2001.

[3] Johannesson P., Svensson T., de Maré J., *An Extension of the Relative Miner Rule*, Chalmers University of Technology, 2004.

[4] Memon I.R., Zhang X., Cui D., *Fatigue life prediction of 3-D problems by damage mechanics with two-block loading*, International Journal of Fatigue, 2001.

[5] Borg W., *High Temperature Low Cycle Fatigue Testing Of A Stainless Steel*, 2004.

[6] Meetham G.W., Van de Voorde M.H., *Materials for High Temperature Engineering Applications*, 2000.

[7] Suresh S., *Fatigue of Materials*, 1998.

[8] Kelly S.M., *Fatigue*, MSE 2094 Class Project, Virginia Tech Materials Science and Engineering, 1997.

[9] Outokumptu, Products and Services, 05/09/05.

`http://www.outokumpu.com/files/Stainless/Documents/Publications/1000EN2_Wall%20chart_Europe.pdf`

[10] Atlas Steels Australia, 05/09/05.

`http://www.atlas-steels.com.au/customer/downloads/technical_handbook/technical_handbook.pdf`

[11] Material Suppliers Online, 05/09/05.

`http://www.suppliersonline.com/propertypages/253MA.asp`

[12] Atlas Steels Australia, 05/09/05.

`http://www.azom.com/Details.asp?ArticleID=959`

[13] Haynes International Inc., 05/09/05.

`http://www.haynesintl.com/H3116ahra/H3116Ap9mp.htm`

[14] Manson S.S., *Fatigue: A Complex Subject - Some simple Aproximations*, Expt. Mech., Vol. 5, 1965.

[15] Landgraft R.W., Morrow J. and Endo T., *Determination of the Cyclic Stress-Strain Curve*, Journal of Materials, ASTM, Vol. 4, No. 1, March, 1969.

[16] American Society for Testing and Materials, ASTM. *Standard Practice for Strain-Controlled Fatigue Testing*, E 606–92 (Reapproved 1998).

[17] Instron Model 8500 plus Dynamic Testing System, Operator's guide, 1995.

[18] Instron WaveMaker Software, Cat. No. 2490-749, User's guide, 1994.

[19] LabVIEW User Manual, National Instruments, 1998.

[20] Entech Energiteknik AB, 15/09/05.

`http://www.entech.se/pdf/Split_furnace_ESTF_11.pdf`

[21] Product Manual MTS 632.53/54 High-Temperature Axial Extensometer, 1995.

[22] Timoshenko S., *Teoría de la Elasticidad*, 1951.

[23] MatLab & Simulink Manual, The MathWorks Inc, 2004.

A. Appendix: Resumen del proyecto

Breve descripción

El presente proyecto se desarrolló en las dependencias de *Lunds Tekniska Högskola*, perteneciente a la Universidad de Lund (Suecia), bajo la dirección y supervisión del Departamento de Materiales de la citada escuela.

El Departamento disponía de una máquina de fatiga Instron recientemente puesta en funcionamiento tras un tiempo en desuso. Para su puesta a punto, se realizó un primer proyecto de fatiga de amplitud constante a alta temperatura. Posteriormente, para lograr un mayor ajuste, se llevó a cabo el presente proyecto basado en la implementación de ensayos de fatiga a alta temperatura y amplitud de carga variable.

A través del análisis de los resultados experimentales, se evaluó la eficacia de la renombrada regla de Palmgren-Miner para el cálculo de daño acumulado. La aplicación de la misma generó predicciones aceptables si bien, en la mayoría de los casos, conservativa.

Profundizando en el estudio de los distintos parámetros influyentes en dicha regla, se desarrollaron distintas curvas de Wöhler o curvas S-N, descubriendo que el uso de la deformación total en la ecuación de Coffin-Manson mejorable notablemente los resultados finales.

Paralelamente al estudio, se analizaron los efectos de ciertos casos particulares: la secuencia de los bloques, los picos de carga y la duración relativa de los bloques

de carga.

Desarrollo

Tras un detallado estudio de la bibliografía sobre el tema, se procedió a la puesta a punto de la maquinaria para la realización de los distintos ensayos. El material utilizado fue acero inoxidable de la clase 253MA, que ya había sido empleado en el proyecto precedente. Tanto las probetas elaboradas como la maquinaria y los procesos implicados en los experimentos, observaban todas las indicaciones de la norma ASTM E606–92 *Standard Practice for Strain-Controlled Fatigue Testing*.

La máquina de ensayos, el horno y el extensómetro se calibraron para ejecutar el plan de ensayos previamente diseñado. Todos los ensayos se realizaron a 700 ℃, 0.5 Hz de frecuencia y bajo una relación de amplitudes R de -1.

Aún siendo la mayoría de experimentos de amplitud variable, también se ensayaron algunas probetas a amplitud constante, con el fin de ampliar el rango de tensiones estudiadas hasta el momento. La fuerza y la deformación soportada por las probetas se recogieron y almacenaron electrónicamente, lo que permitió el cálculo de distintas magnitudes de utilidad.

Una vez finalizada la etapa experimental se procedió al análisis de los resultados. En primer lugar, los datos disponibles de estudios anteriores se compararon con los recogidos en este proyecto, con el objeto de verificar su validez y justificar su uso en lo sucesivo. A continuación, se obtuvo la curva de comportamiento cíclico del material pudiéndose observar un claro endurecimiento cíclico si bien, la composición de los fenómenos transitorios en los ensayos de amplitud variable presentaban cierta complejidad.

Predicciones de vida a fatiga. Regla de Palmgren-Miner. El principal objetivo del proyecto consistía en un estudio de fiabilidad de la regla de Palmgren-Miner para el cálculo del daño acumulado. Para ello, las vidas a fatiga obtenidas en los ensayos debían ser contrastadas con las proporcionadas por dicha regla.

Para la aplicación de la citada regla era necesaria la deducción previa de la vida a fatiga en un nivel de carga de amplitud constante. Esto se consiguió a través de la curva basada en la ecuación de Coffin-Manson,

$$\frac{\Delta\epsilon_p}{2} = \epsilon'_f(2N_f)^c,$$

que relacionaba la deformación plástica con el número de ciclos hasta el fallo. Las deformaciones plásticas usadas en este cómputo se obtuvieron a través de una curva de conversión de deformación total a deformación plástica.

Una vez obtenidas las predicciones y comparadas con los datos experimentales, se constató que las razones entre ambos se encontraban entre los límites habituales en todos los casos. Una característica común a todas las probetas, con sólo una excepción, era el carácter conservativo de las previsiones, especialmente a alta carga.

A pesar de que los resultados se consideraron aceptables, el hecho de que el pronóstico para alta carga fuese sensiblemente diferente al de baja carga, sugería una posible dependencia del comportamiento del material del nivel de carga aplicado. En este caso, la curva basada en la ecuación de Coffin-Manson, desarrollada para baja carga, podía estar introduciendo un error inherente en alta carga.

Con el fin de aclarar la sospecha, dos nuevas probetas se ensayaron a amplitud constante a alta carga, confirmando el cambio de comportamiento en este rango

de amplitudes. A consecuencia de este hallazgo, se desarrollaron dos modelos alternativos de la curva de fatiga a amplitud constante.

Curvas alternativas para amplitud constante. La distinta respuesta a diferentes niveles de carga indicaba que la deformación elástica jugaba un papel importante. Por este motivo se propuso un modelo basado en la deformación total, descrito por la siguiente ecuación:

$$\frac{\Delta\epsilon}{2} = \frac{\sigma'_f}{E}(2N_f)^b + \epsilon'_f(2N_f)^c.$$

Tras sustituir la ecuación de Coffin-Manson por esta nueva, se apreció una notable mejoría en los resultados, especialmente a niveles altos de carga. El carácter conservativo de las predicciones, aunque en menor grado, seguía presente en todas salvo una de las muestras.

Sin embargo, los ensayos se habían llevado a cabo bajo condiciones de fatiga de bajo ciclo, en la que la deformación elástica debería tener una influencia despreciable. Esta contradicción condujo al planteamiento de un nuevo modelo de curva, basado únicamente en la deformación plástica, ahora descompuesta en dos sumandos:

$$\frac{\Delta\epsilon_p}{2} = \frac{\sigma'_f}{E}(2N_f)^b + \epsilon'_f(2N_f)^c.$$

Nuevamente se produjo una mejoría con respecto a los resultados originales si bien, menor que en el caso anterior. La curva de la deformación plástica, descompuesta en dos términos, apenas se diferenciaba de la inicial, ya que uno de ellos era despreciable frente al otro.

Casos particulares Durante la realización de los ensayos, se observó que probetas sometidas a configuraciones de carga similares respondían de manera distinta. Esto propició el seguimiento de ciertos casos particulares. Se analizaron así los efectos de la variación de la secuencia de los bloques, de los picos de carga y de la duración relativa de los bloques de carga.

En el caso de probetas sometidas a bloques de carga de igual amplitud pero distinta duración relativa entre ambos, se apreció una disminución de la vida al reducir la duración del bloque de nivel elevado de carga. Por otro lado, la variación de la secuencia de los bloques de carga parecía influir cuantiosamente en la resistencia de la muestra. En todos los casos, la aplicación del bloque de carga alta en primer lugar causaba una rotura anterior a la producida si se aplicase en segundo lugar.

Conclusiones

El principal objetivo de reajuste y puesta en funcionamiento de la máquina de fatiga, había sido alcanzado a través de la implementación de una serie de ensayos a alta temperatura y carga variable.

El estudio de fiabilidad de la regla de de Palmgren-Miner para el cálculo del daño acumulado constató valía de la regla para la estimación de la vida a fatiga del acero 253MA a 700 ℃. A lo largo de este estudio, se observaron los efectos de tres casos particulares: secuencia de los bloques, de los picos de carga y de la duración relativa de los bloques de carga. Los datos experimentales mostraron cómo dichos casos afectaban a la vida de las probetas.

Este análisis hizo patentes dos claras debilidades de la citada regla: una fuerte

dependencia del enfoque elegido para amplitud constante así como la ausencia de términos que reflejen los casos particulares descritos anteriormente.

Por último, se apreció que la ecuación de Coffin-Manson fallaba en zonas de carga elevada. De las distintas propuestas alternativas, se concluyó que el modelo basado en la deformación total era el que proporcionaba mejores resultados.

B. Appendix: Software scripts and programs

Several programs and software written in MatLab were developed for this thesis. The scripts are collected hereby.

Generation of the hysteresis plots

```
[filn,pt]=uigetfile('*.*','Load');
d=load(strcat(pt,filn));
A=31.65; %area de la probeta
F=d(:,2);
ep=d(:,3);
si=F*1000/A;
t=d(:,1)-d(1,1);

figure(1)
clf
plot(ep,si)
grid
xlabel('\epsilon (%)')
ylabel('\sigma (MPa)')

figure(2)
clf
plot(t,si);
hold on
xlabel('t (s)')
ylabel('\sigma (MPa)')
grid

figure(3)
clf
plot(t,ep);
grid
xlabel('t (s)')
ylabel('\epsilon (%)');
```

Calculation of Young's Modulus, Elastic, Plstic and Total Strains

```
clear all
[filn,pt]=uigetfile('*.*','Load the file');
chico=load(strcat(pt,filn));
cd('C:\Documents and Settings\Carmen\Mis documentos\Documentos...
  ... Carmen\Thesis\samples')
h=1;%sample 1
diam=load('diametros.txt');
d0=diam(h);
cd ..

Area=d0*d0*3.1416/4;
F=chico(:,2);
ep=chico(:,3);
si=F*1000/Area;
t=chico(:,1)-chico(1,1);

figure(1)
clf
plot(ep,si)
hold on
grid
xlabel('\epsilon (%)')
ylabel('\sigma (MPa)')
AXIS([min(ep)-0.1 max(ep)+0.1 min(si)-140 max(si)+60])

k=0;
epmax=max(ep);
simax=max(si);
x=[si(27) ep(27); si(31) ep(31)];
k=((x(2,1)-x(1,1))/(x(2,2)-x(1,2)));
E=(k*100*1e+6*1e-9);

siffra=round(E);
test=['Youngs Modul (E) = ' num2str(siffra) 'GPa'];
title(test,'FontSize',12)
A(h,1)=siffra;
```

```
epmin=min(ep);
simin=min(si);
m=x(2,1)-k*x(2,2);
korsep1=(simin-m)/k;
korsep2=(simax-m)/k;

plot(x(1,2),x(1,1),'ro',x(2,2),x(2,1),'ro')
linje1x=[korsep1 korsep2];
linje1y=[simin simax];
plot(linje1x,linje1y,'r-',linje1x,linje1y,'ro')

linje2x=[epmin korsep1 korsep2];
linje2y=[simin simin simin];
plot(linje2x,linje2y,'r-',linje2x,linje2y,'ro')

linje3x=[korsep2 korsep2];
linje3y=[simax simin];
plot(linje3x,linje3y,'r-',linje3x,linje3y,'ro')

deltaeps=korsep2-epmin;
siffra=round(deltaeps*1000)/1000;
test=['\Delta\epsilon = ' num2str(siffra)];
text(korsep1+0.07,simin+35,num2str(test),'FontSize',12)
A(h,3)=siffra;

deltaepsp=korsep1-epmin;
siffra=round(deltaepsp*1000)/1000;
test=['\Delta\epsilon_{p} = ' num2str(siffra)];
text(epmin+(korsep1-epmin)/4,simin-90,num2str(test),'FontSize',12)
A(h,4)=siffra;

deltaepse=korsep2-korsep1;
siffra=round(deltaepse*1000)/1000;
test=['\Delta\epsilon_{e} = ' num2str(siffra)];
text(epmax-(epmax-korsep1)/1.5,simin-90,num2str(test),...
     ...'FontSize',12)
A(h,5)=siffra;
dlmwrite('sa1.xls',A,'\t')
```

Generation of the Cyclic Stress Strain Curve (CSS)

```
clear all
a=[];
b=[];
f=1;
for p=1:1:16
    if p~=9
    u=num2str(p);
    cd(char(strcat('C:\Documents and Settings\Carmen\...
       ...Mis documentos\Documentos Carmen\Thesis\...
       ...samples\chicocss\',u)));
    d=dir;
    for z=1:1:(length(d)-2);
        w=num2str(z);
        cd(char(strcat('C:\Documents and Settings\Carmen\...
           ...Mis documentos\Documentos Carmen\Thesis\...
           ...samples\chicocss\',u,'\',w)));
        d1=dir('*.txt');
        entera=[];
        for k=1:1:length(d1)
            j=num2str(k);
            name=char(strcat('chico',u,'-',w,'-',j,'.txt'));
            parte=load(name);
            entera(length(entera)+1:length(entera)...
                   ...+length(parte),:)=parte;
        end
        cd ..
        cd ..
        cd ..

        diam=load('diametros.txt');
        d0=diam(p);
        Area=d0*d0*3.1416/4;
        F=entera(:,2);
        si=F*1000/Area;

        k=0;
        b=0;
        c=0;
```

```
        m=0;
        maxims=[];
        maximsneg=[];
        aux=[];
        for i=2:1:length(si)
            if (si(i)>0 & si(i)>si(i-1))
                k=k+1;
                aux(k,1)=si(i);
                aux(k,2)=entera(i,3);
            end
            if (si(i)<0 & si(i-1)<=0 & k>0)
                b=b+1;
                maxims(b,1)=max(aux(:,1));
                maxims(b,2)=max(aux(:,2));
                aux=[];
                k=0;
            end
            if (si(i)<0 & si(i)<si(i-1))
                m=m+1;
                aux(m,1)=si(i);
                aux(m,2)=entera(i,3);
            end
            if (si(i)>0 & si(i-1)>=0 & m>0)
                c=c+1;
                maximsneg(c,1)=min(aux(:,1));
                maximsneg(c,2)=min(aux(:,2));
                aux=[];
                m=0;
            end
        end
        maximos(f,1)=mean(maxims(:,1));
        maximos(f,2)=mean(maxims(:,2));
        length(maxims)
        minimos(f,1)=mean(maximsneg(:,1));
        minimos(f,2)=mean(maximsneg(:,2));
        length(maximsneg)
        f=f+1;
    end
    end
end
plot(maximos(:,2),maximos(:,1),'*')
```

```
hold on
plot(minimos(:,2),minimos(:,1),'*')
primer6=load('primer6.txt');
F6=primer6(:,2);
d6=diam(6);
Area6=d6*d6*3.1416/4;
si6=F6*1000/Area;
e6=primer6(:,3);
plot(e6,si6,'r')
```

Prediction of lifetime at constant amplitude loading (Coffin-Manson relationship)

```
figure
clf
walterep=[0.596 .577 .448 .377 .315 .257 .119 .184 .536 .202 .156];
walterN=[1175 1125 1581 1394 2122 3425 11675 8445 1090 3094 13626];
wep=log(.01.*walterep');
wN=log(walterN');
w=walterep.*0.01;
X=[ones(length(wN),1),wN];
b=regress(wep,X)
n=10^3:100:2*10^4;
loglog(n,0.2502./n.^0.5566,'b')
hold on
loglog(walterN,w,'o')
hold on
loglog(n,exp(b(1))./n.^-b(2),'r')
Vida=[1/b(2) -b(1)/b(2)]; %y=b1+b2x
datos=log(0.01.*eplastica); %definir la deformacion antes
casi=polyval(Vida,datos);
prediccion=exp(casi);
fprintf('%4.0f\n',prediccion)
```

Prediction of cumulative fatigue lifetime (Coffin-Manson relationship)

```
function [a,b]= predict()
Z=[500 100 1145 451
100 500 451 1145
100 1 669 451
1 100 451 669
100 10 1145 451
100 50 1145 451
50 100 451 1145
100 100 6705 1909
100 10 6705 1909
100 100 6705 1909
100 1 6705 1909
100 100 6705 1909];
a1=Z(:,1);
a2=Z(:,2);
N1=Z(:,3);%vida a amplitud constante
N2=Z(:,4);%vida a amplitud constante

for h=1:1:12
    a=0;
    b=0;
    j=1;
    for i=1:10000;
        if (a/N1(h) +b/N2(h))>=1;
            break
        end
        a=a+1;
        if a==a1(h)*j;
           for g=1:10000;
               b=b+1;
               if (a/N1(h) +b/N2(h))>=1;
                  break
               end
               if b==a2(h)*j;
                  j=j+1;
                  break
               end
```

```
            end
         end
      end
      A(h,1)=a;
      A(h,2)=b;
      fprintf('(sample%2.0f) Expected life 1 =%5.0f cycles\n',h,a)
      fprintf('Expected life 2 =%5.0f cycles\n',b)
end
dlmwrite('expectedlife.xls',A,'\t')
```

Prediction of lifetime by the three alternative curves

```
%Total strain approach
y=[0.0028
0.0065
0.0080
0.0050
0.0040
0.0025];

x0=[5951
460
500
882
1636
9095]*2;

g=inline('0.379*x.^(-0.6323)+0.005011*x.^(-0.1149)-0.01*0.28');
Nf(1)=fzero(g,x0(1));
g=inline('0.379*x.^(-0.6323)+0.005011*x.^(-0.1149)-0.65*0.01');
Nf(2)=fzero(g,x0(2));
g=inline('0.379*x.^(-0.6323)+0.005011*x.^(-0.1149)-0.80*0.01');
Nf(3)=fzero(g,x0(3));
g=inline('0.379*x.^(-0.6323)+0.005011*x.^(-0.1149)-0.50*0.01');
Nf(4)=fzero(g,x0(4));
g=inline('0.379*x.^(-0.6323)+0.005011*x.^(-0.1149)-0.40*0.01');
Nf(5)=fzero(g,x0(5));
g=inline('0.379*x.^(-0.6323)+0.005011*x.^(-0.1149)-0.25*0.01');
```

```
Nf(6)=fzero(g,x0(6));
x=500:100:30000;
loglog(x,0.379*x.^(-0.6323)+0.005011*x.^(-0.1149),'b')
hold on
loglog(Nf,y,'b*')

%Coffin-Manson curve
yp=0.01*[0.198
0.824
1.074
0.574
0.407
0.157]/2;
loglog(x,0.2502./(2*(x/2).^0.5566),'g')
m=inline('exp((log(2*(t/0.2502)))/(-0.5566)+log(2))');
Nf2=feval(m,yp);
loglog(Nf2,yp,'g*')

%Combined plastic strain approach
g=inline('0.1983*x.^(-0.5526)+9.459*x.^(-4.866)-0.00099');
Nf3(1)=fzero(g,x0(1));
g=inline('0.1983*x.^(-0.5526)+9.459*x.^(-4.866)-0.00412');
Nf3(2)=fzero(g,x0(2));
g=inline('0.1983*x.^(-0.5526)+9.459*x.^(-4.866)-0.00537');
Nf3(3)=fzero(g,x0(3));
g=inline('0.1983*x.^(-0.5526)+9.459*x.^(-4.866)-0.00287');
Nf3(4)=fzero(g,x0(4));
g=inline('0.1983*x.^(-0.5526)+9.459*x.^(-4.866)-0.002035');
Nf3(5)=fzero(g,x0(5));
g=inline('0.1983*x.^(-0.5526)+9.459*x.^(-4.866)-0.000785');
Nf3(6)=fzero(g,x0(6));
loglog(x,0.1983*x.^(-0.5526)+9.459*x.^(-4.866),'k')
loglog(Nf3,yp,'k*')

Z=[500 100
100 500
100 1
1 100
100 10
100 50
50 100
```

```
100 100
100 10
100 100
100 1
100 100
500 100
100 500 ];

a1=Z(:,1);
a2=Z(:,2);

for k=1:1:3;
    if k==1;
        aux=Nf';
        name='Total';
    elseif k==2;
        aux=Nf2';
        name='Coffin';
    elseif k==3;
        aux=Nf3';
        name='Combined';
    end
    N1=[aux(4) aux(3) aux(2) aux(3) aux(4)*ones(1,2)...
        ...aux(3) aux(6)*ones(1,6) aux(5)]'/2;
    N2=[aux(3) aux(4) aux(3) aux(2) aux(3)*ones(1,2)...
        ...aux(4) aux(5)*ones(1,6) aux(6)]'/2;
    for h=1:1:14
        a=0;
        b=0;
        j=1;
        for i=1:10000;
            if (a/N1(h) +b/N2(h))>=1;
               break
            end
            a=a+1;
            if a==a1(h)*j;
               for g=1:10000;
                   b=b+1;
                   if (a/N1(h) +b/N2(h))>=1;
                      break
                   end
```

```
                    if b==a2(h)*j;
                       j=j+1;
                       break
                    end
                 end
              end
           end
       A(h,1)=a;
       A(h,2)=b;
   end
   filename=[name,'predictions.xls'];
   dlmwrite(filename,A,'\t')
end
```

Calculation of the stresses

```
[filn,pt]=uigetfile('*.*','Load the file');
parte=load(strcat(pt,filn));
prompt = {'Number of sample'};
dlg_title = 'Number specimen';
num_lines= 1;
answer  = inputdlg(prompt,dlg_title,num_lines);
ab=str2double(answer);
h=ab(1);
cd('C:\Documents and Settings\Carmen\Mis documentos\...
   ...Documentos Carmen\Thesis\samples')
diam=load('diametros.txt');
cd ..
d0=diam(h);
Area=d0*d0*3.1416/4;
F=parte(:,2);
si=F*1000/Area;
```

Calculation of the average of the maximum stresses

```
function [a]=meanmax(si)
k=0;
b=0;
maxims=[];
aux=[];
for i=2:1:length(si)
    if (si(i)>0 & si(i)>si(i-1))
        k=k+1;
        aux(k)=si(i);
    end
    if (si(i)<0 & si(i-1)<=0 & k>0)
        b=b+1;
        maxims(b)=max(aux);
        k=0;
    end
end
a=mean(maxims)
```

Routine to split the files from the loggin machine

```
[filn,pt]=uigetfile('*.*','Load');
d=load(strcat(pt,filn));
prompt = {'Size of the file:','number of specimen'}; %Megas
dlg_title = 'Number of files';
num_lines= 1;
answer  = inputdlg(prompt,dlg_title,num_lines);
ab=str2double(answer);
t=ceil(ab(1)/1.2);
for i=1:t
    j=num2str(i)
    name=char(strcat('s',answer(2),'-',j,'.doc'));
    fid=fopen(name,'w');
    fprintf(fid,'%12.3f\t%+5.3f\t%+5.3f\n',...
      ..d(ceil((i-1)*length(d)/t)+1:ceil(i*length(d)/t),:)');
    fclose(fid)
```

```
end
```

Routine to reassemble the files from the loggin machine

```
prompt = {'Number of files','number of specimen'};
dlg_title = 'Number of files';
num_lines= 1;
answer  = inputdlg(prompt,dlg_title,num_lines);
ab=str2double(answer);
t=ab(1);
aux=[];
for i=1:t
    j=num2str(i);
    name=char(strcat('s',answer(2),'-',j,'.doc'));
    aux2=load(name);
    aux(length(aux)+1:length(aux)+length(aux2),:)=aux2;
end
nombre=char(strcat('s',answer(2),'.doc'));
fid=fopen(nombre,'w');
    fprintf(fid,'%12.3f\t%+5.3f\t%+5.3f\n',aux');
    fclose(fid);
```

C. Appendix: Compendium of Results and Calculations

The outcomes of the calculations performed in this thesis are presented in this appendix along with the results of the experiments.

First approach: Coffin-Manson relationship

The initial approach was based on the Coffin-Manson relationship. The most important data generated for this section are collected in the following table:

Sam	N_B	$\Delta\epsilon/2$	$\Delta\epsilon_p$	$2N_f$	N_p	N_r	N_{pT}	N_{rT}	N_{rT}/N_{pT}
	First Block						Complete Test		
1		0.275	0.198	11936			5968	3479	0.6
2		0.40	0.407	3271			1636	1745	1.1
3	500	0.50	0.574	1763	574	1077	674	1277	1.9
4	100	0.80	1.074	572	124	195	624	912	1.5
5	100	0.65	0.824	921	455	800	459	808	1.8
6	1	0.80	1.074	572	5	8	458	708	1.5
7	100	0.50	0.574	1763	697	1100	757	1210	1.6
8	100	0.50	0.574	1763	400	700	557	1050	1.9
9	50	0.80	1.074	572	189	300	489	800	1.6
10	100	0.25	0.157	18109	1400	1816	2783	3616	1.3
11	100	0.25	0.157	18109	5844	5051	6424	5551	0.9
12	100	0.25	0.157	18109	1400	1800	2783	3578	1.3
13	100	0.25	0.157	18109	8584	10322	8669	10425	1.2
14	100	0.25	0.157	18109	1400	1400	2783	2729	1.0
15		0.80	1.074	572			286	629	2.2
16		0.50	0.574	1763			882	1350	1.5
	Second Block								
3	100	0.80	1.074	572	100	200			
4	500	0.50	0.574	1763	500	500			
5	1	0.80	1.074	572	4	8			
6	100	0.65	0.824	921	453	700			
7	10	0.80	1.074	572	60	110			
8	50	0.80	1.074	572	157	350			
9	100	0.50	0.574	1763	300	500			
10	100	0.40	0.407	3271	1383	1800			
11	10	0.40	0.407	3271	580	500			
12	100	0.40	0.407	3271	1383	1778			
13	1	0.40	0.407	3271	85	103			
14	100	0.40	0.407	3271	1383	1329			

Table C.1: Initial approach based on Coffin-Manson relationship. (Sam: Sample number; N_B: Number of cycles of the block; $\Delta\epsilon/2$: Total strain amplitude [%]; $\Delta\epsilon_p$: Plastic strain range [%]; $2N_f$: Number of load reversals to failure; N_p: Predicted number of cycles at the block loading level; N_r: Real number of cycles at the block loading level; N_{pT}: Predicted lifetime; N_{rT}: Experimental lifetime; N_{rT}/N_{pT}: Ratio between predicted and experimental lifetime.)

Second approach: Total Strain approach

The second approach used the total strain amplitude in the development of the constant amplitude curve. The most important data generated for this section are collected in the following table:

Sam	N_B	$\Delta\epsilon/2$	$\Delta\epsilon_p$	$2N_f$	N_p	N_r	N_{pT}	N_{rT}	N_{rT}/N_{pT}
	First Block						Complete Test		
1		0.275	0.198	14628			7314	3479	0.5
2		0.40	0.407	3971			1986	1745	0.9
3	500	0.50	0.574	2132	756	1077	856	1277	1.5
4	100	0.80	1.074	686	183	195	683	912	1.3
5	100	0.65	0.824	1108	546	800	551	808	1.5
6	1	0.80	1.074	686	6	8	551	708	1.3
7	100	0.50	0.574	2132	818	1100	898	1210	1.3
8	100	0.50	0.574	2132	445	700	645	1050	1.6
9	50	0.80	1.074	686	215	300	615	800	1.3
10	100	0.25	0.157	22261	1700	1816	3383	3616	1.1
11	100	0.25	0.157	22261	7151	5051	7861	5551	0.7
12	100	0.25	0.157	22261	1700	1800	3383	3578	1.1
13	100	0.25	0.157	22261	10000	10322	10100	10425	1.0
14	100	0.25	0.157	22261	1700	1400	3383	2729	0.8
15		0.80	1.074	686			343	629	1.8
16		0.50	0.574	2132			1066	1350	1.3
	Second Block								
3	100	0.80	1.074	686	100	200			
4	500	0.50	0.574	2132	500	500			
5	1	0.80	1.074	686	5	8			
6	100	0.65	0.824	1108	545	700			
7	10	0.80	1.074	686	80	110			
8	50	0.80	1.074	686	200	350			
9	100	0.50	0.574	2132	400	500			
10	100	0.40	0.407	3971	1683	1800			
11	10	0.40	0.407	3971	710	500			
12	100	0.40	0.407	3971	1683	1778			
13	1	0.40	0.407	3971	100	103			
14	100	0.40	0.407	3971	1683	1329			

Table C.2: Second approach based on the total strain amplitude. (Sam: sample number; N_B: Number of cycles of the block; $\Delta\epsilon/2$: Total strain amplitude [%]; $\Delta\epsilon_p$: Plastic strain range [%]; $2N_f$: Number of load reversals to failure; N_p: Predicted number of cycles at the block loading level; N_r: Real number of cycles at the block loading level; N_{pT}: Predicted lifetime; N_{rT}: Experimental lifetime; N_{rT}/N_{pT}: Ratio between predicted and experimental lifetime.)

Third approach: Combined plastic strain approach

The last approach considered that the elastic strain was negligible in the development of the constant amplitude curve. This method used a double term formula for the definition of the plastic strain. The most important data generated for this section are collected in the following table:

Sam	N_B	$\Delta\epsilon/2$	$\Delta\epsilon_p$	$2N_f$	N_p	N_r	N_{pT}	N_{rT}	N_{rT}/N_{pT}
	First Block						Complete Test		
1		0.275	0.198	11328			5664	3479	0.6
2		0.40	0.407	3824			1912	1745	0.9
3	500	0.50	0.574	2188	811	1077	911	1277	1.4
4	100	0.80	1.074	771	200	195	727	912	1.3
5	100	0.65	0.824	1200	593	800	598	808	1.4
6	1	0.80	1.074	771	6	8	597	708	1.2
7	100	0.50	0.574	2188	867	1100	947	1210	1.3
8	100	0.50	0.574	2188	500	700	710	1050	1.5
9	50	0.80	1.074	771	245	300	645	800	1.2
10	100	0.25	0.157	15565	1600	1816	3119	3616	1.2
11	100	0.25	0.157	15565	5544	5051	6094	5551	0.9
12	100	0.25	0.157	15565	1600	1800	3119	3578	1.1
13	100	0.25	0.157	15565	7482	10322	7556	10425	1.4
14	100	0.25	0.157	15565	1600	1400	3119	2729	0.9
15		0.80	1.074	771			386	629	1.6
16		0.50	0.574	2188			1094	1350	1.2
	Second Block								
3	100	0.80	1.074	771	100	200			
4	500	0.50	0.574	2188	527	500			
5	1	0.80	1.074	771	5	8			
6	100	0.65	0.824	1200	591	700			
7	10	0.80	1.074	771	80	110			
8	50	0.80	1.074	771	210	350			
9	100	0.50	0.574	2188	400	500			
10	100	0.40	0.407	3824	1519	1800			
11	10	0.40	0.407	3824	550	500			
12	100	0.40	0.407	3824	1519	1778			
13	1	0.40	0.407	3824	74	103			
14	100	0.40	0.407	3824	1519	1329			

Table C.3: Combined plastic strain approach. (Sam: sample number; N_B: Number of cycles of the block; $\Delta\epsilon/2$: Total strain amplitude [%]; $\Delta\epsilon_p$: Plastic strain range [%]; $2N_f$: Number of load reversals to failure; N_p: Predicted number of cycles at the block loading level; N_r: Real number of cycles at the block loading level; N_{pT}: Predicted lifetime; N_{rT}: Experimental lifetime; N_{rT}/N_{pT}: Ratio between predicted and experimental lifetime.)

D. Appendix: Figures from the experiments

The data obtained from the experiments were continuously logged so that the force and the strain undergone by the samples could be further use. After the testing, four plots were generated for every sample: Stress vs. Strain, Hysteresis curve, Stress vs. Time and Strain vs. Time. These plots were used for tracking the experiment's progress once ended. For this reason, the plots have not been cleaned, so that the reader is provided with a real overview of the experiment.

Sample 1

Note: Sample tested before the alignment.

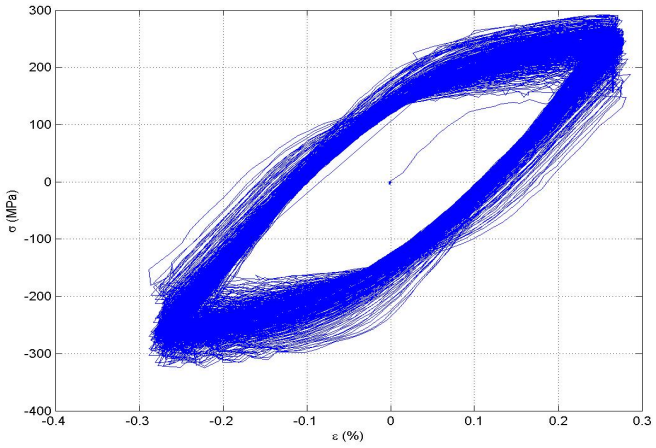

Figure D.1: Hysteresis Curve

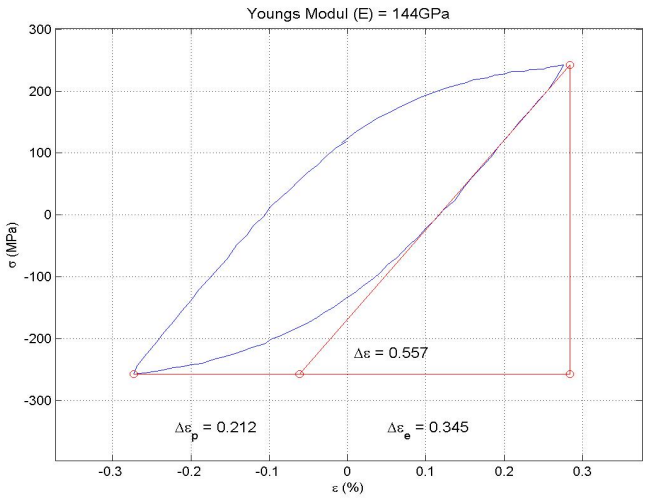

Figure D.2: Hysteresis Curve: Young's Modulus

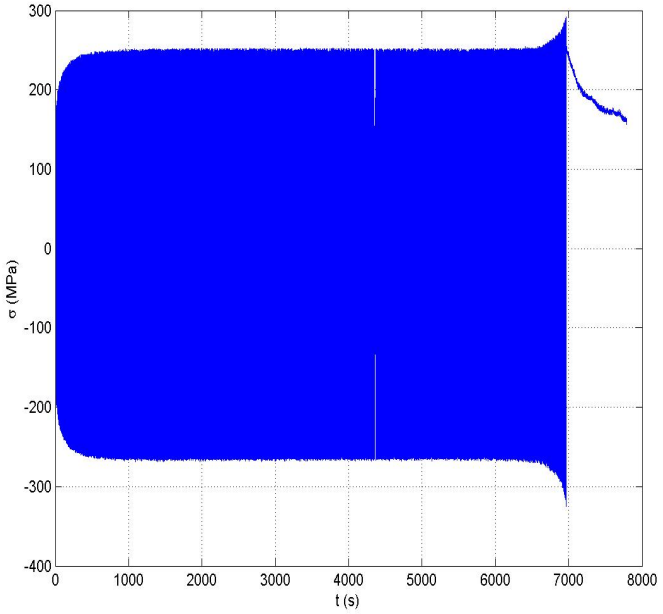

Figure D.3: Stress versus Time

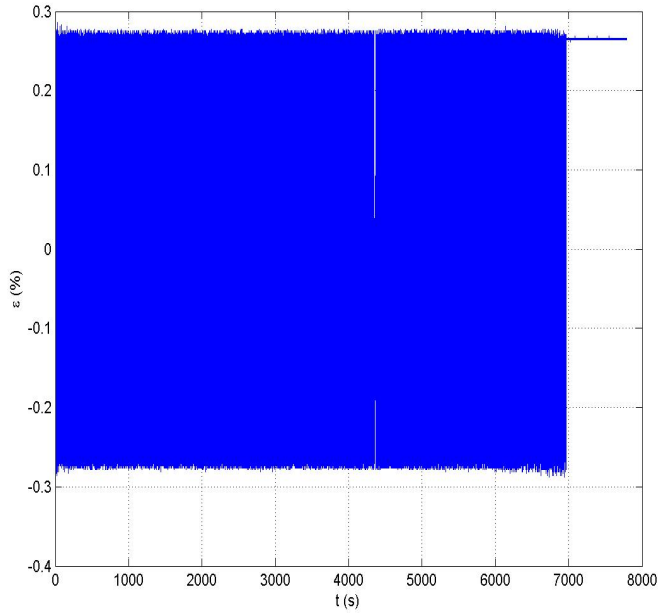

Figure D.4: Strain versus Time

Sample 2

No anomalies registered

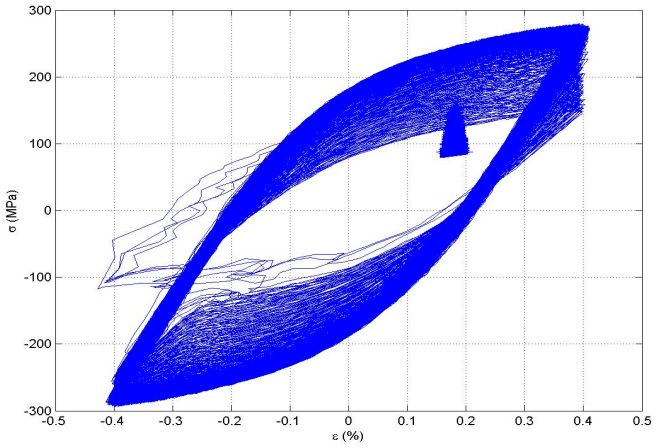

Figure D.5: Hysteresis Curve

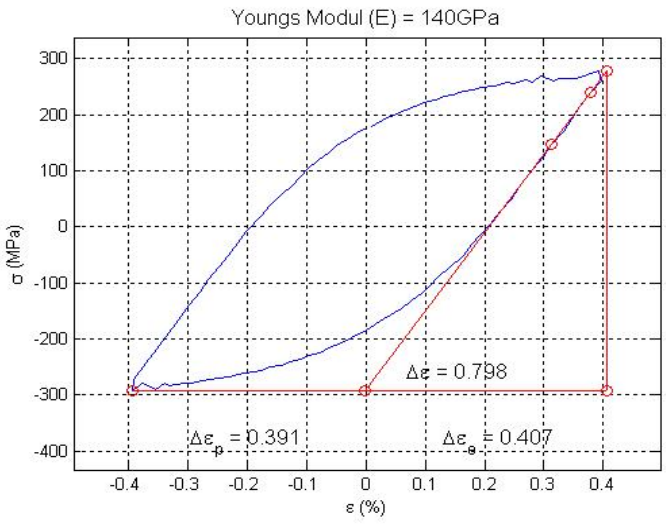

Figure D.6: Hysteresis Curve: Young's Modulus

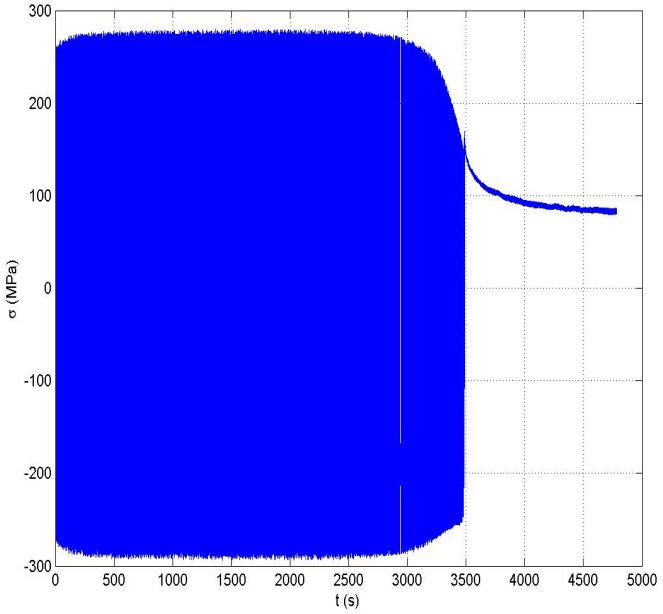

Figure D.7: Stress versus Time

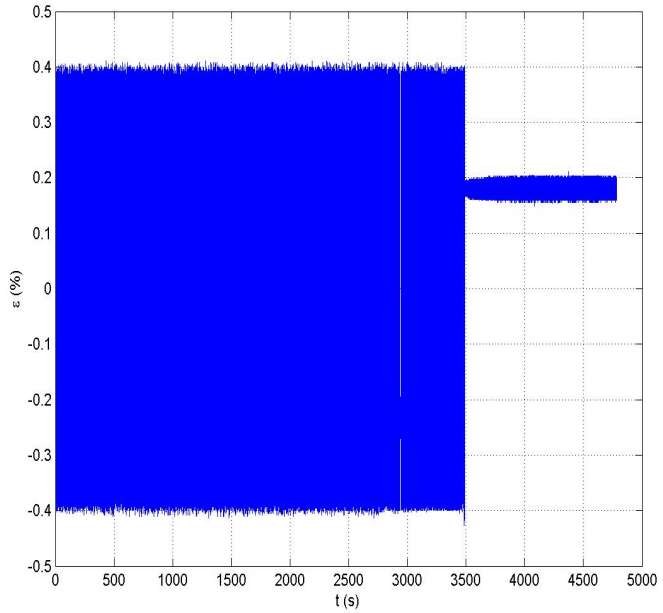

Figure D.8: Strain versus Time

Sample 3

The test was stopped due to the slip of the extensometer rods. The test continued with no incidences.

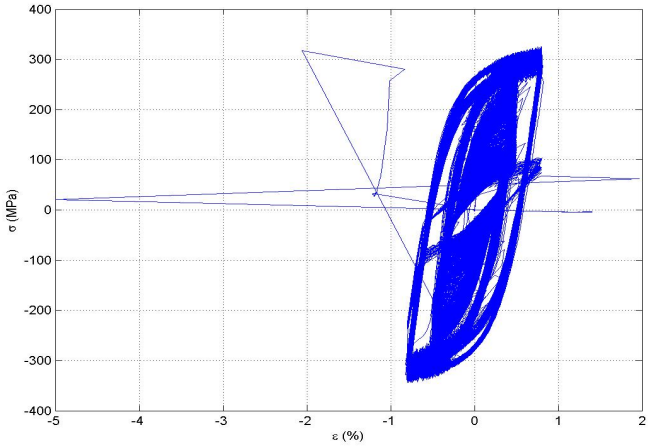

Figure D.9: Hysteresis Curve

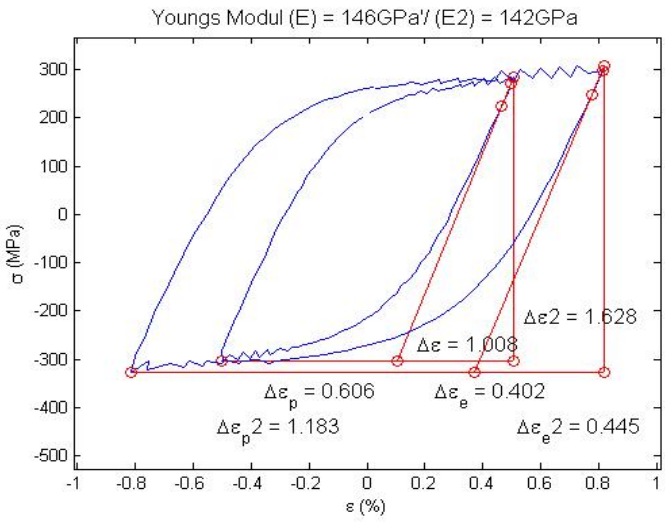

Figure D.10: Hysteresis Curve: Young's Modulus

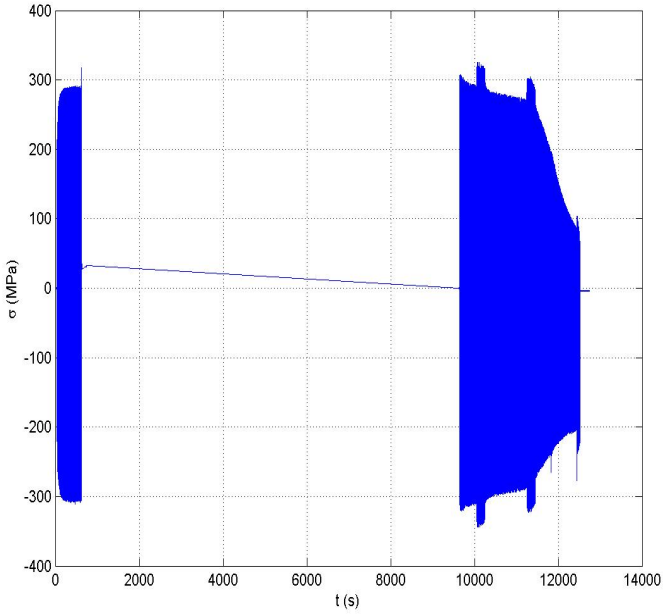

Figure D.11: Stress versus Time

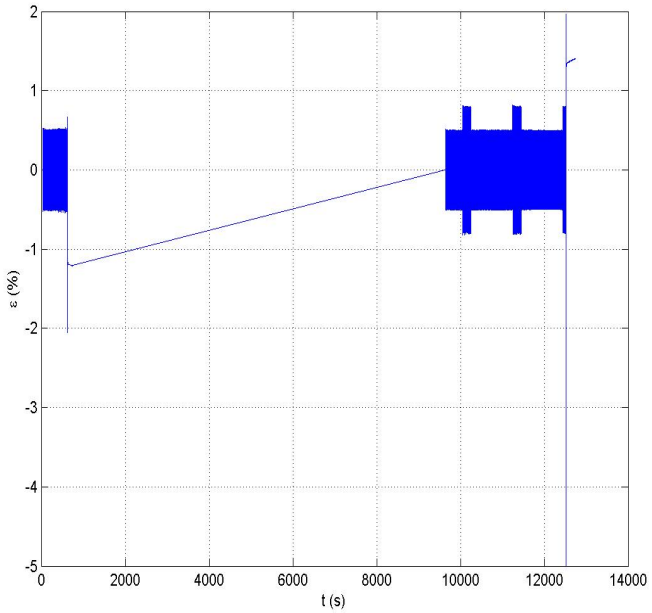

Figure D.12: Strain versus Time

Sample 4

No anomalies registered.

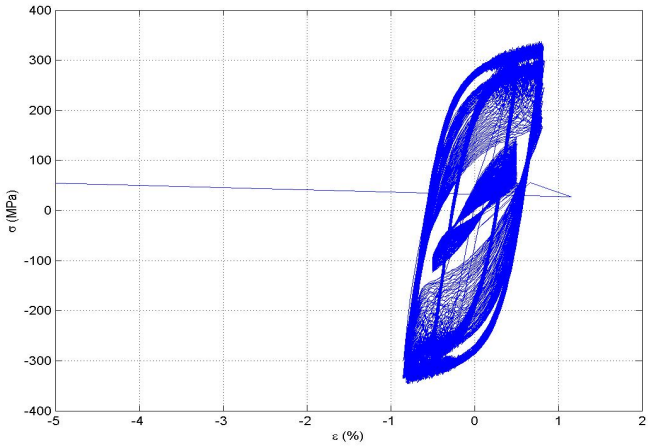

Figure D.13: Hysteresis Curve

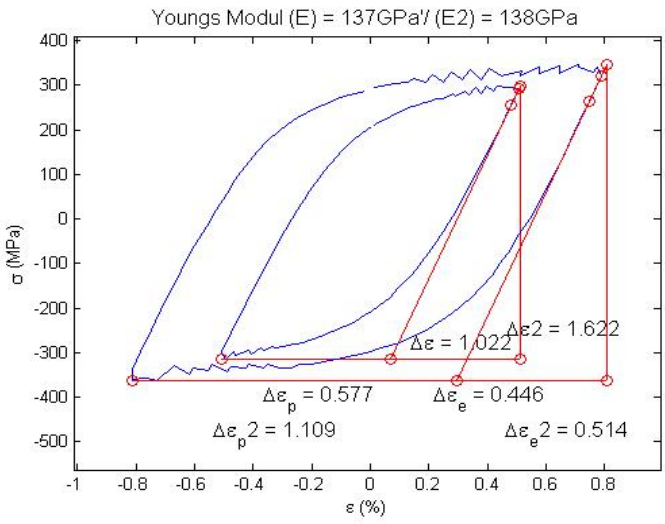

Figure D.14: Hysteresis Curve: Young's Modulus

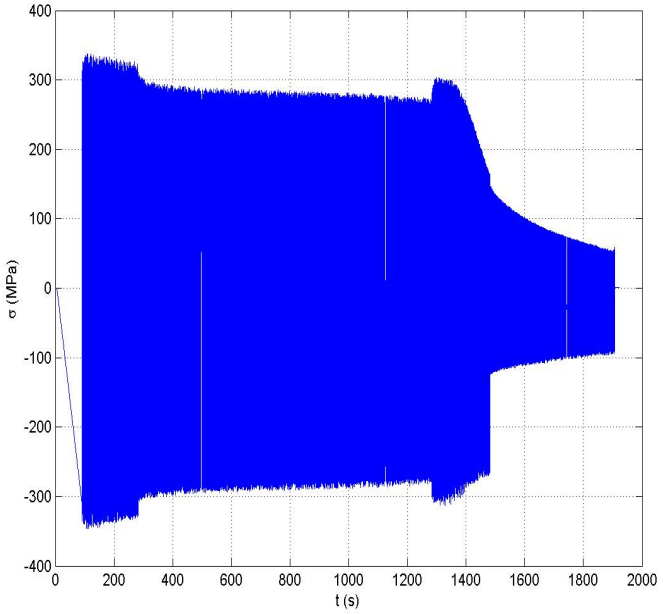

Figure D.15: Stress versus Time

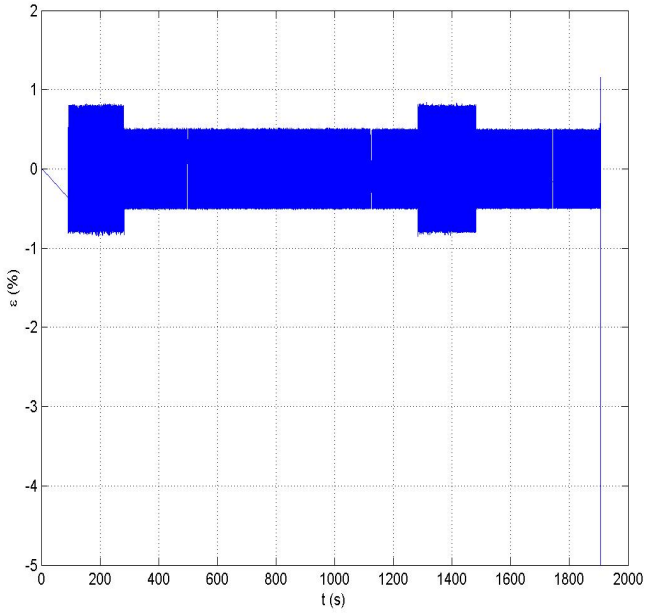

Figure D.16: Strain versus Time

Sample 5

No anomalies registered.

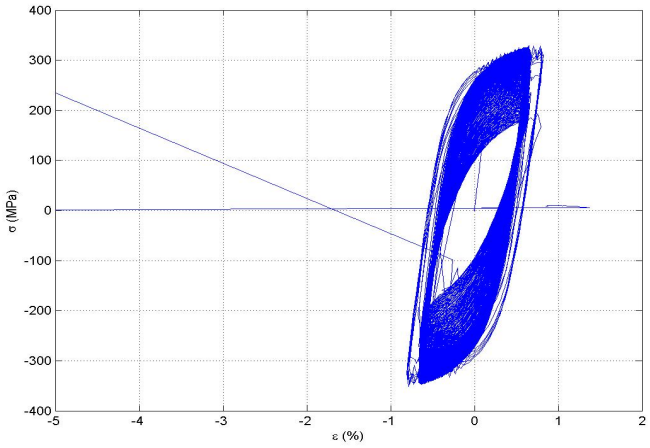

Figure D.17: Hysteresis Curve

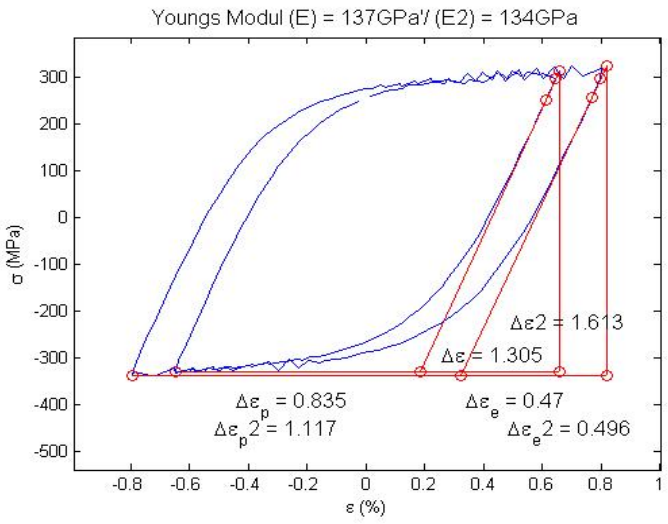

Figure D.18: Hysteresis Curve: Young's Modulus

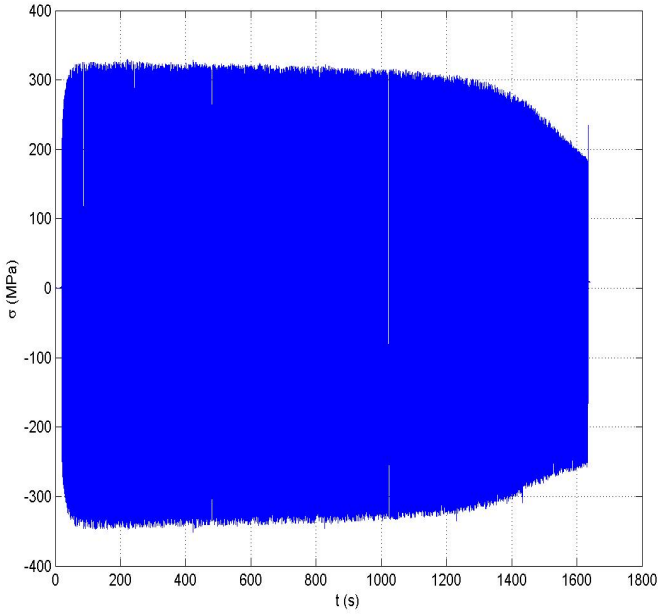

Figure D.19: Stress versus Time

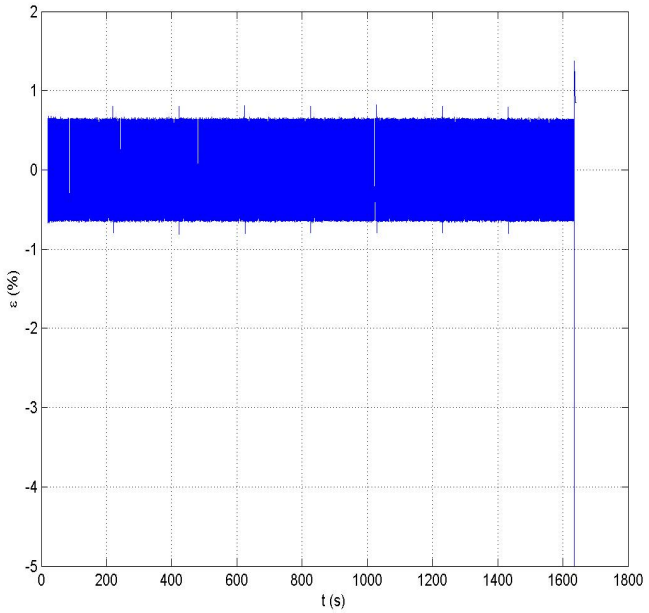

Figure D.20: Strain versus Time

Sample 6

Interferences produced by a static testing machine running close by.

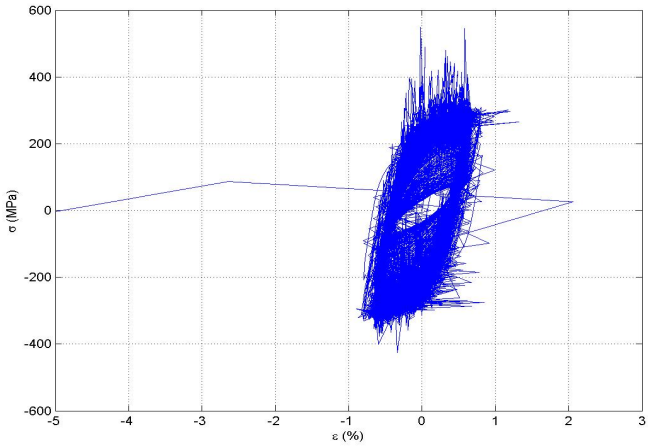

Figure D.21: Hysteresis Curve

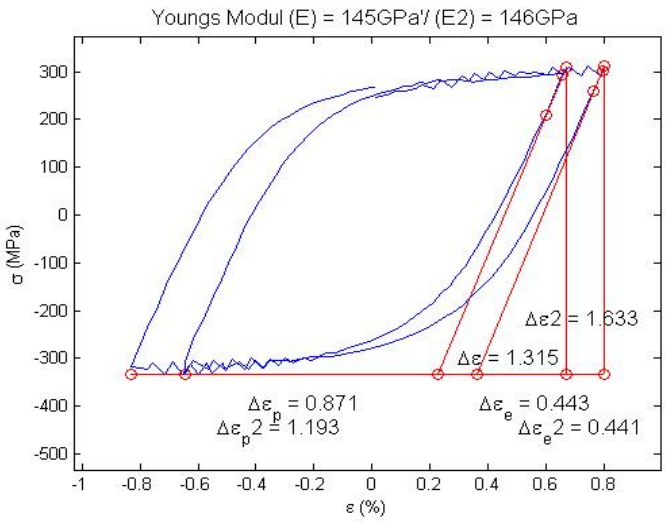

Figure D.22: Hysteresis Curve: Young's Modulus

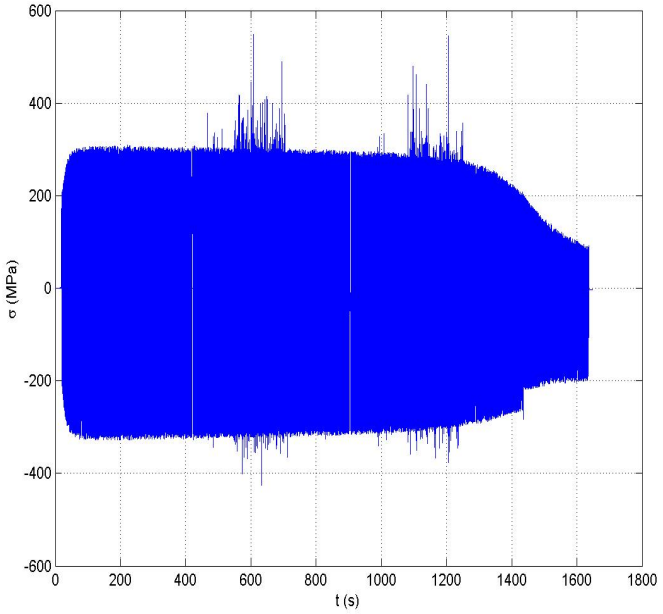

Figure D.23: Stress versus Time

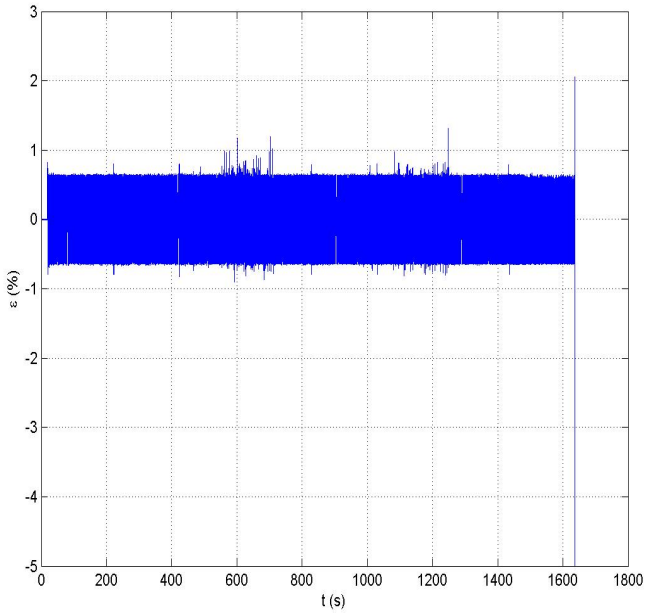

Figure D.24: Strain versus Time

Sample 7

No anomalies registered.

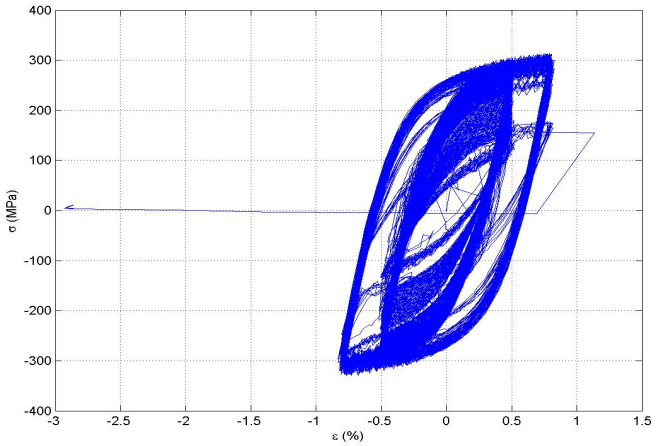

Figure D.25: Hysteresis Curve

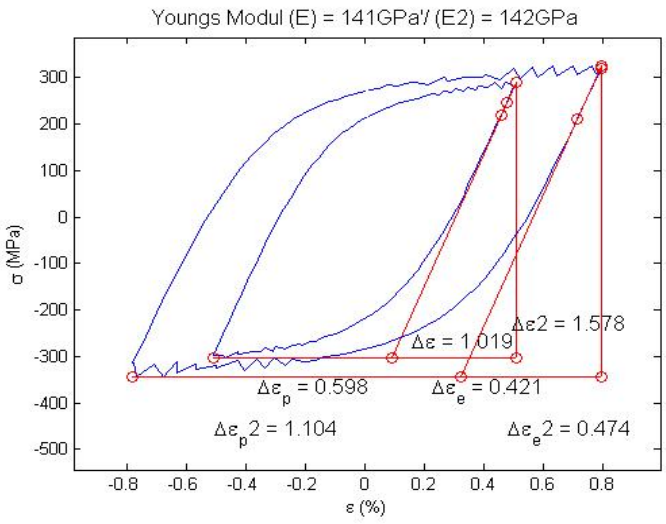

Figure D.26: Hysteresis Curve: Young's Modulus

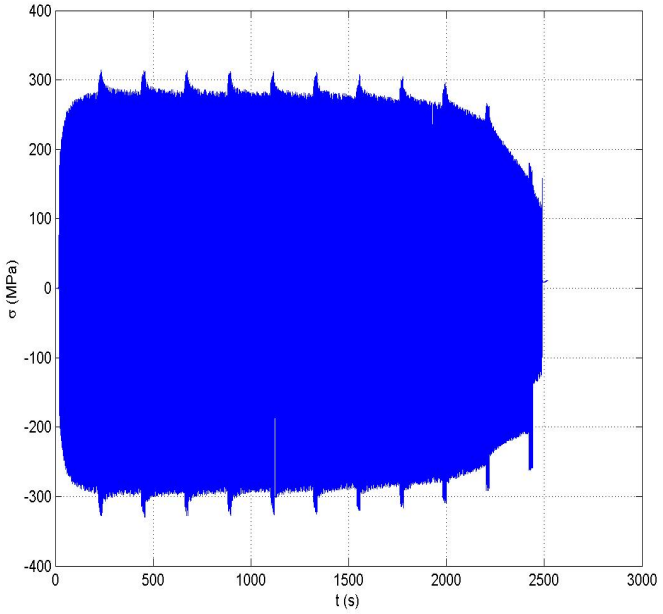

Figure D.27: Stress versus Time

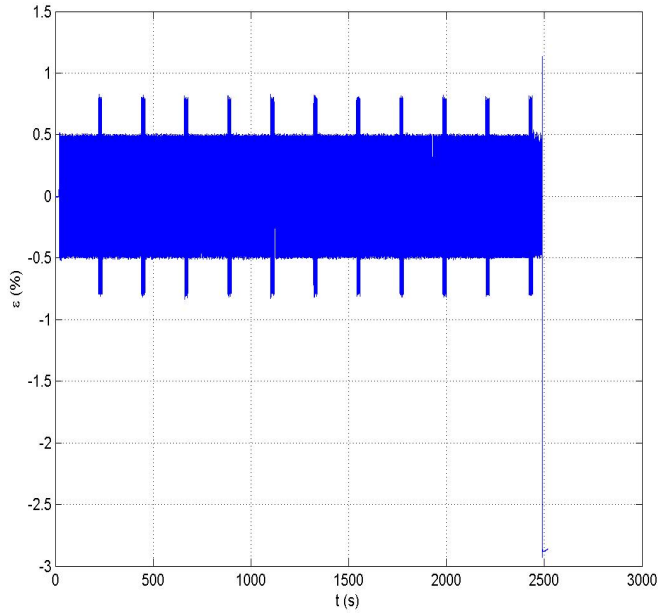

Figure D.28: Strain versus Time

Sample 8

No anomalies registered.

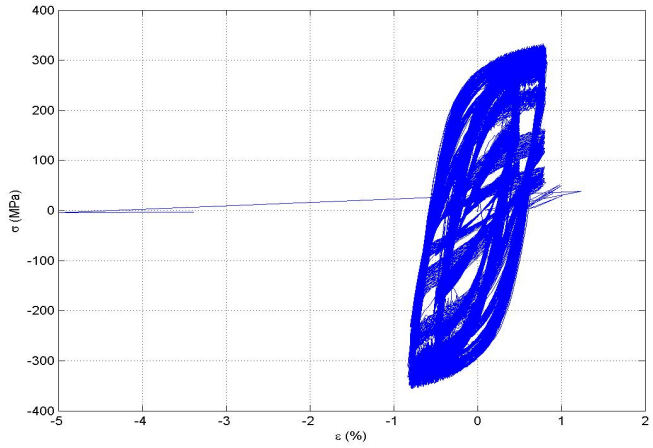

Figure D.29: Hysteresis Curve

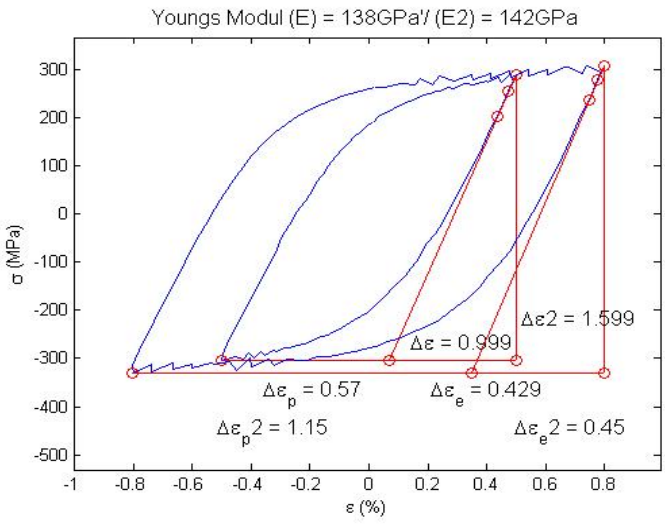

Figure D.30: Hysteresis Curve: Young's Modulus

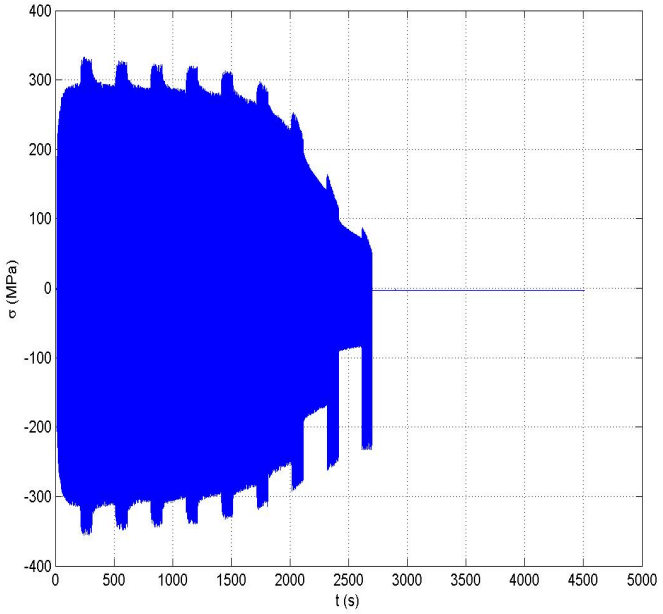

Figure D.31: Stress versus Time

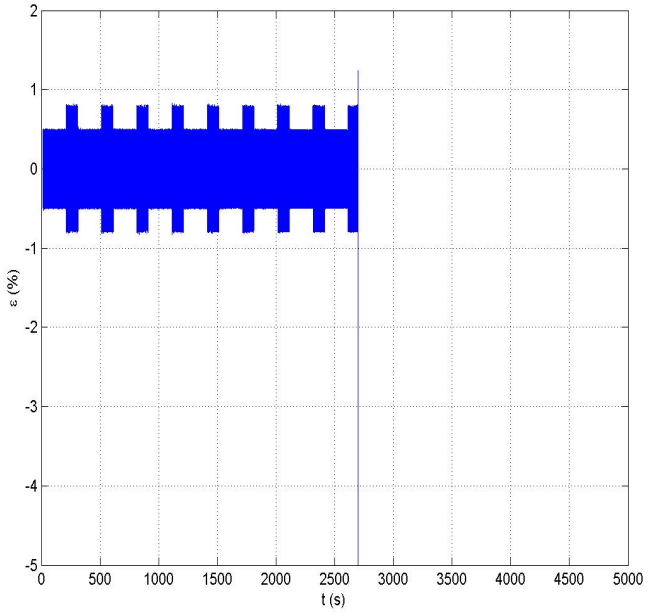

Figure D.32: Strain versus Time

Sample 9

The test was stopped twice due to a mistake in the Instron WaveMaker Software. The test continued with no incidences.

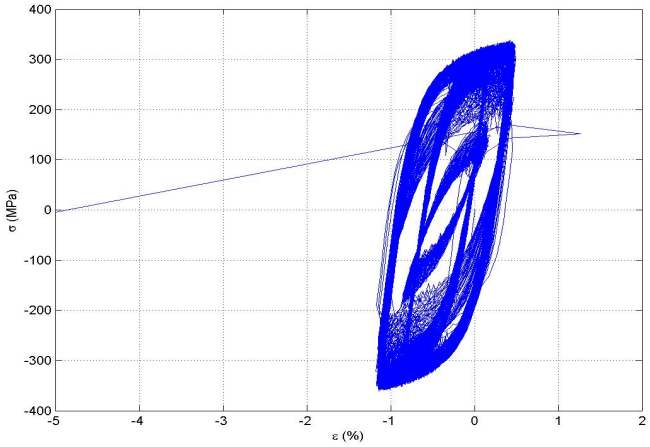

Figure D.33: Hysteresis Curve

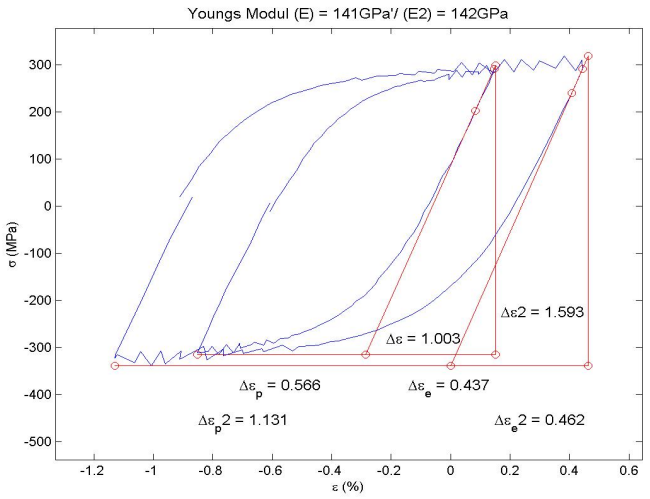

Figure D.34: Hysteresis Curve: Young's Modulus

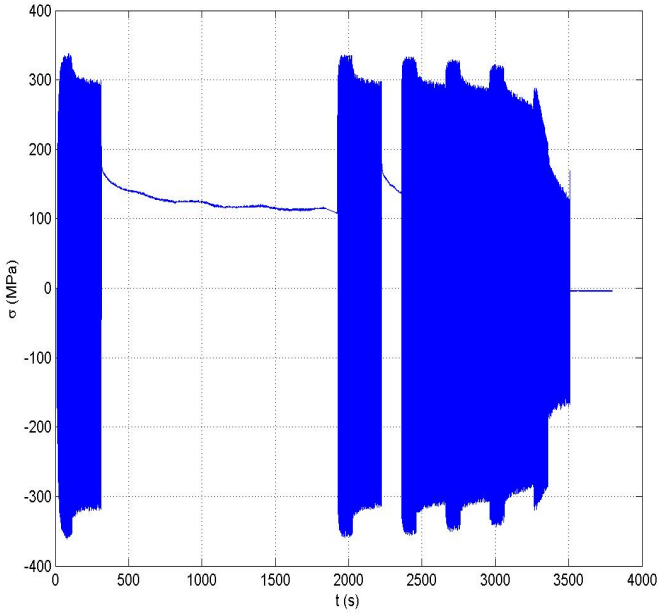

Figure D.35: Stress versus Time

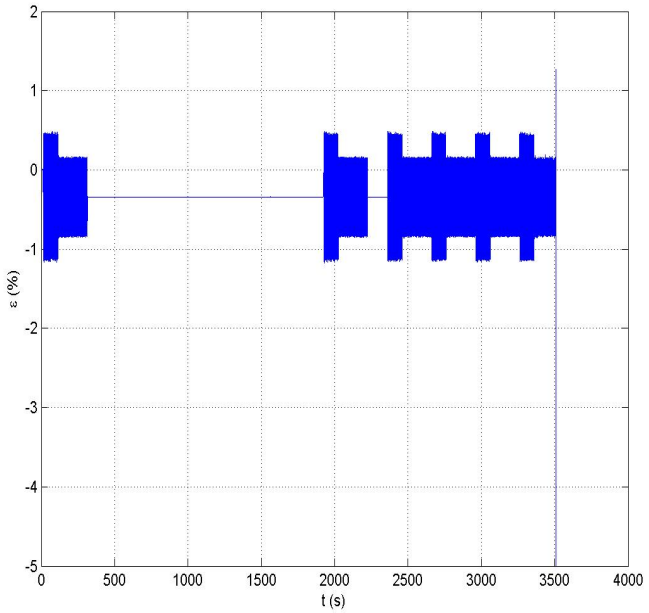

Figure D.36: Strain versus Time

Sample 10

No anomalies registered.

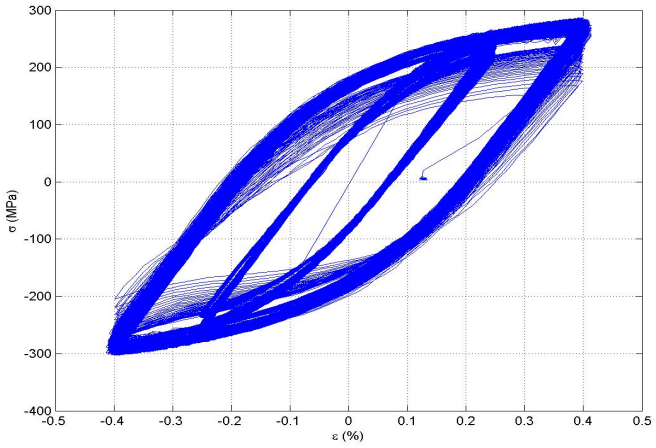

Figure D.37: Hysteresis Curve

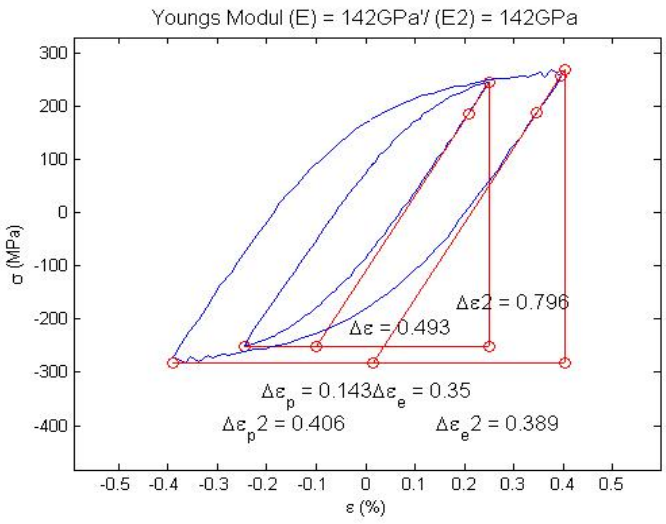

Figure D.38: Hysteresis Curve: Young's Modulus

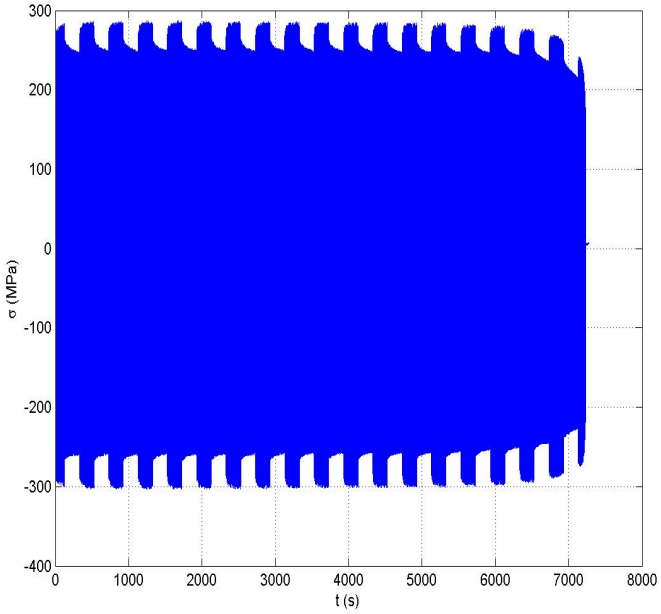

Figure D.39: Stress versus Time

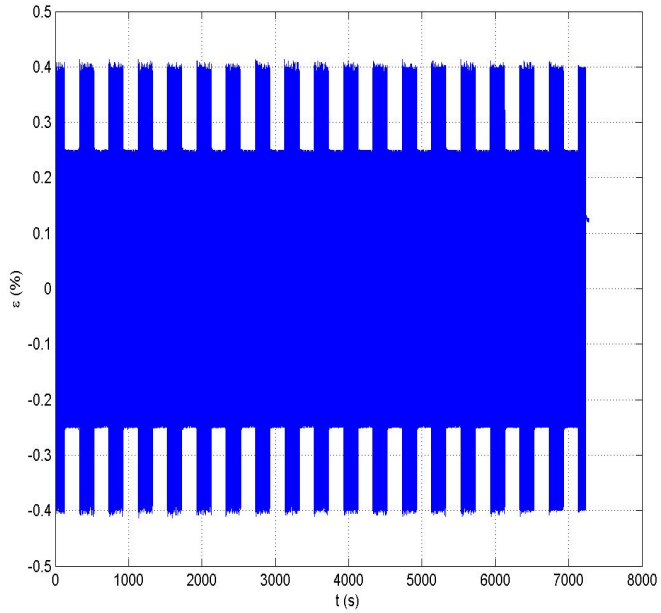

Figure D.40: Strain versus Time

Sample 11

The test was stopped due to the slip of the extensometer rods. The test continued with no incidences.

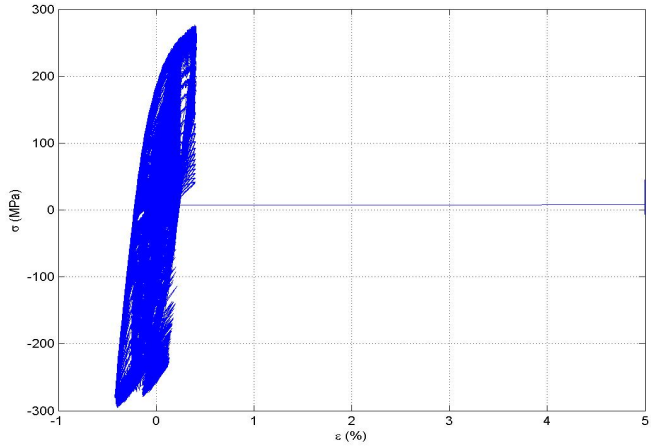

Figure D.41: Hysteresis Curve

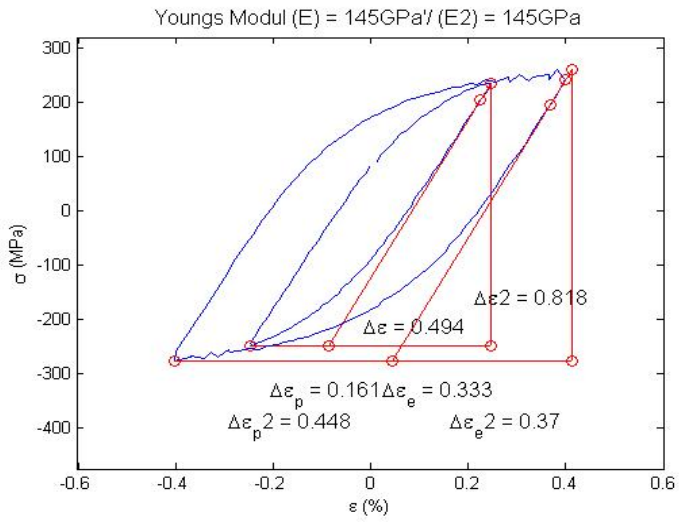

Figure D.42: Hysteresis Curve: Young's Modulus

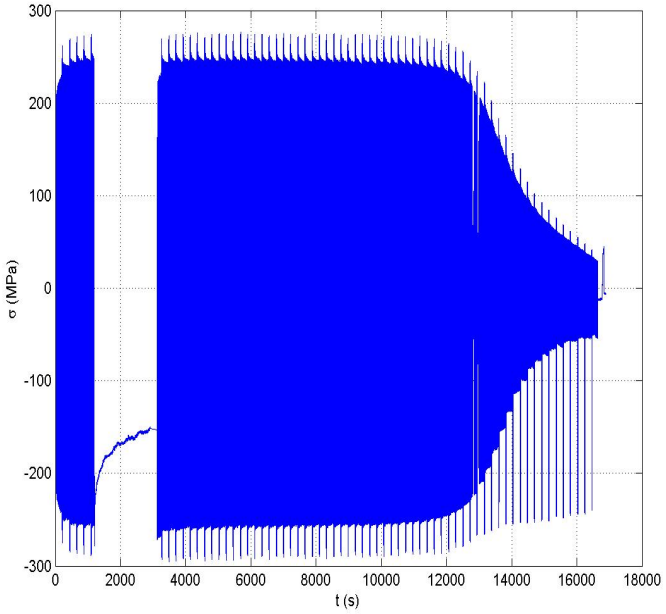

Figure D.43: Stress versus Time

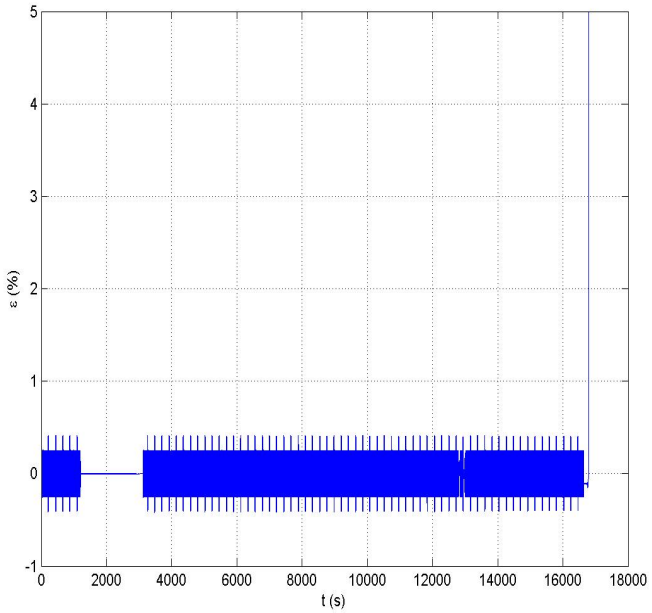

Figure D.44: Strain versus Time

Sample 12

The test was stopped due to the slip of the extensometer rods. The test continued with no incidences.

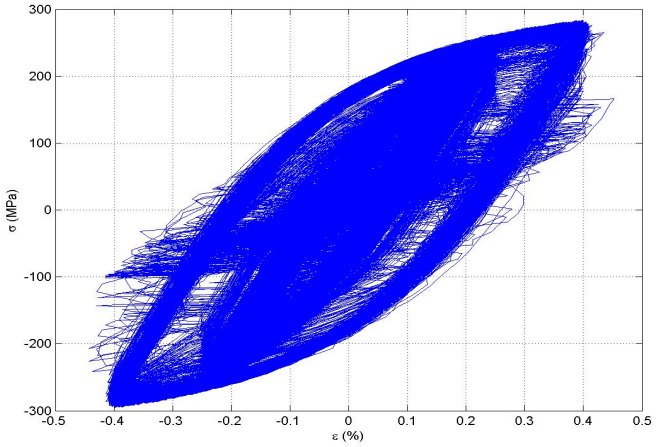

Figure D.45: Hysteresis Curve

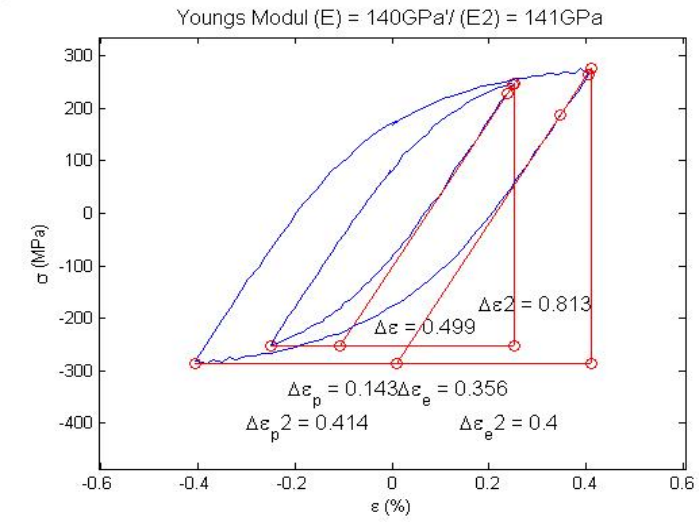

Figure D.46: Hysteresis Curve: Young's Modulus

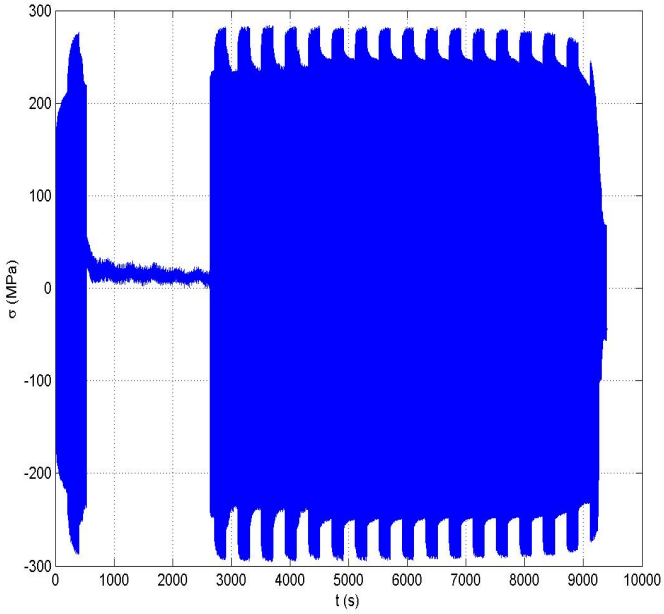

Figure D.47: Stress versus Time

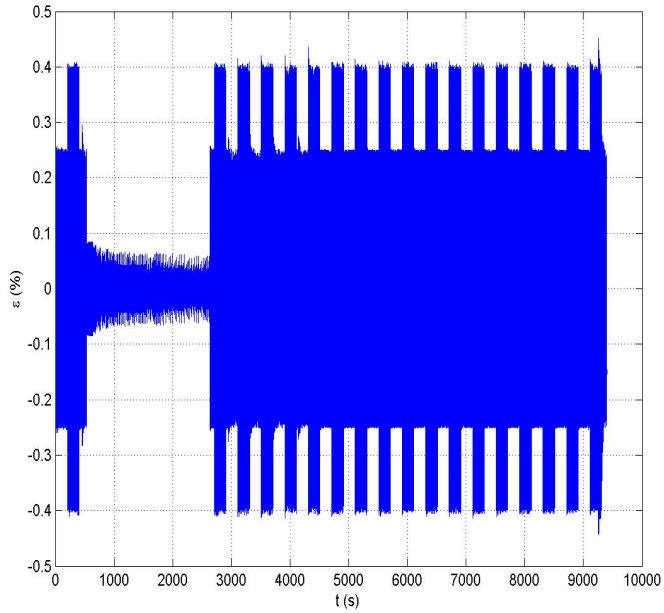

Figure D.48: Strain versus Time

Sample 13

Small interferences produced by a static testing machine running close by.

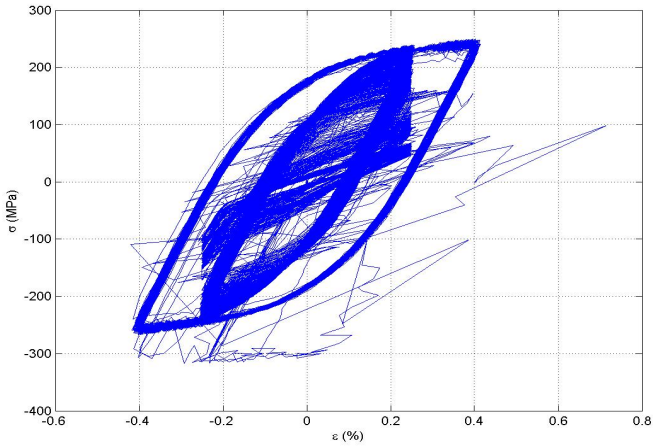

Figure D.49: Hysteresis Curve

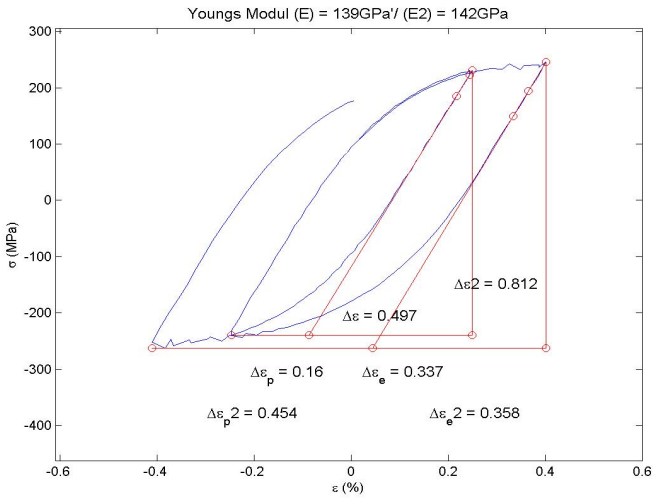

Figure D.50: Hysteresis Curve: Young's Modulus

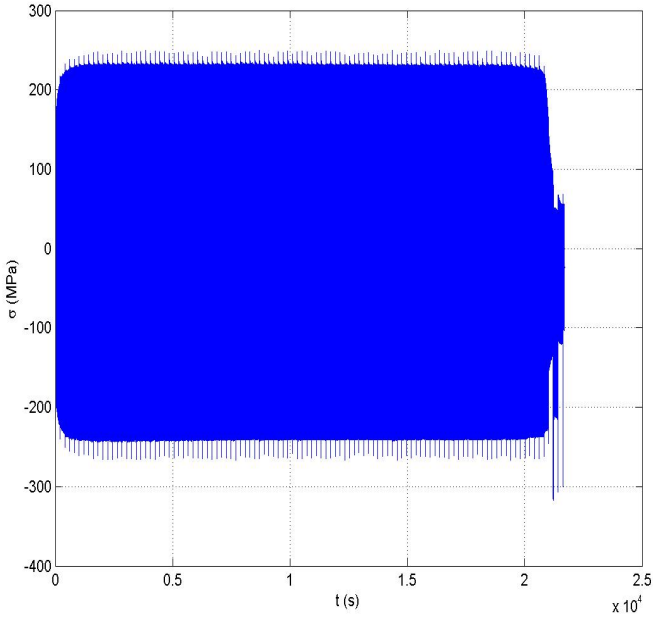

Figure D.51: Stress versus Time

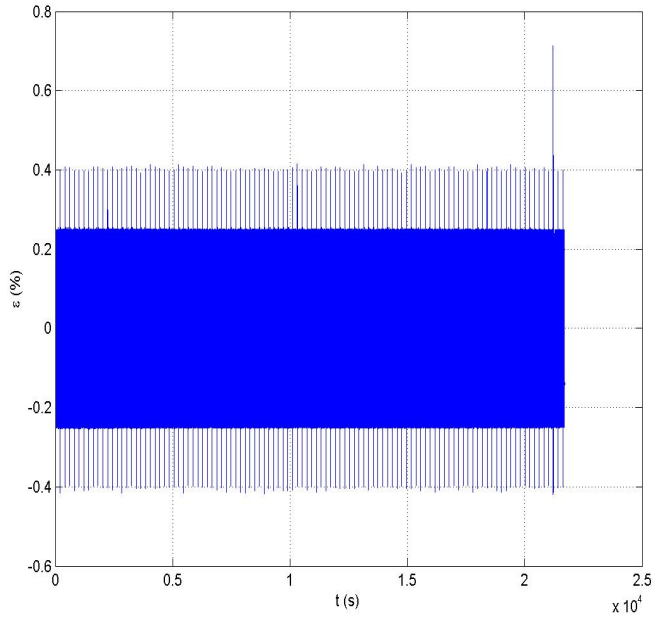

Figure D.52: Strain versus Time

Sample 14

Interferences produced by a static testing machine running close by.

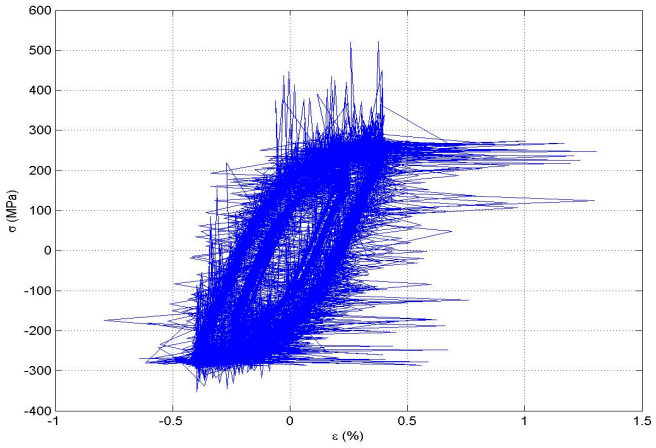

Figure D.53: Hysteresis Curve

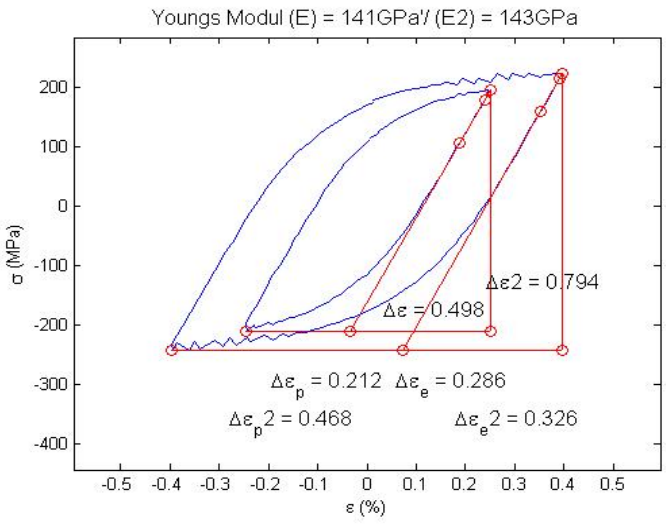

Figure D.54: Hysteresis Curve: Young's Modulus

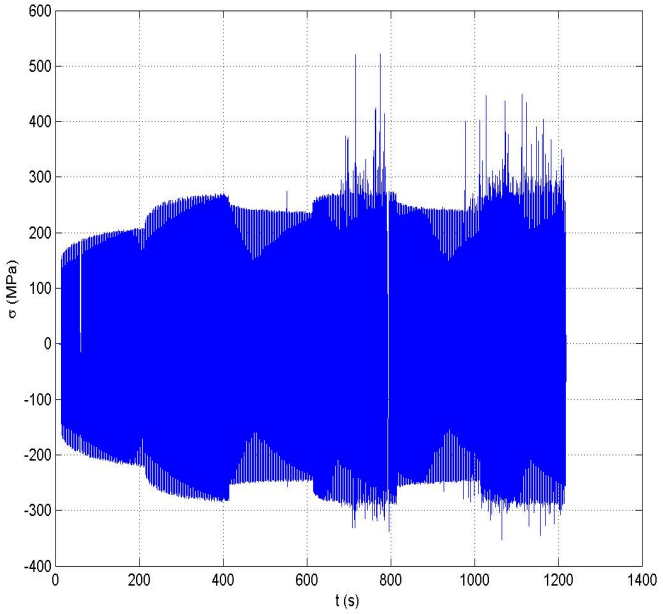

Figure D.55: Stress versus Time

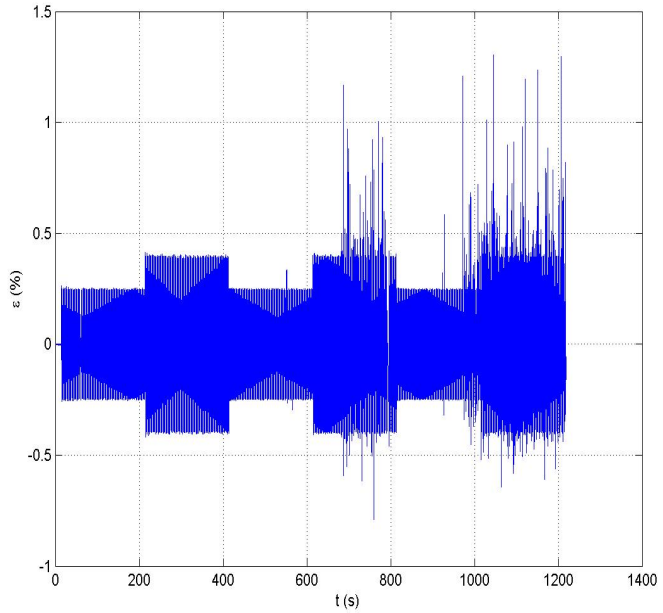

Figure D.56: Strain versus Time

Sample 15

Interferences produced by a static testing machine running close by.

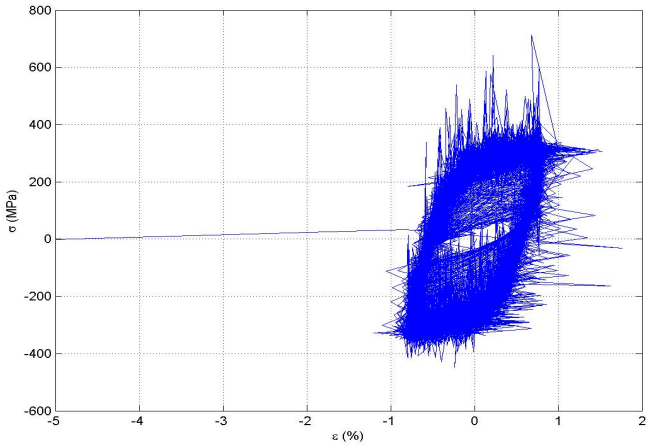

Figure D.57: Hysteresis Curve

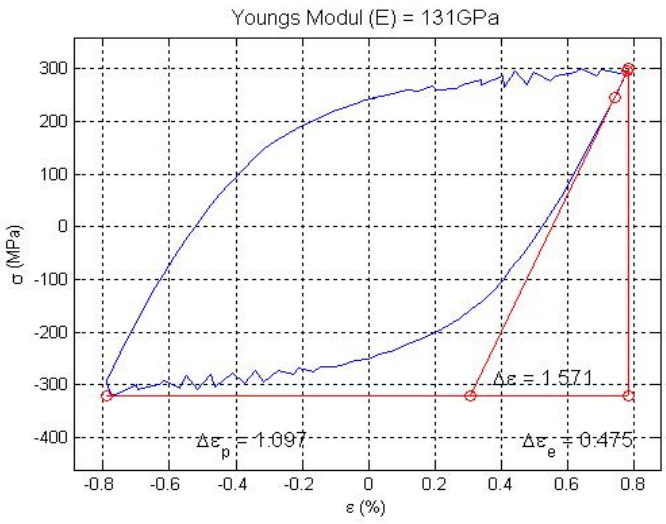

Figure D.58: Hysteresis Curve: Young's Modulus

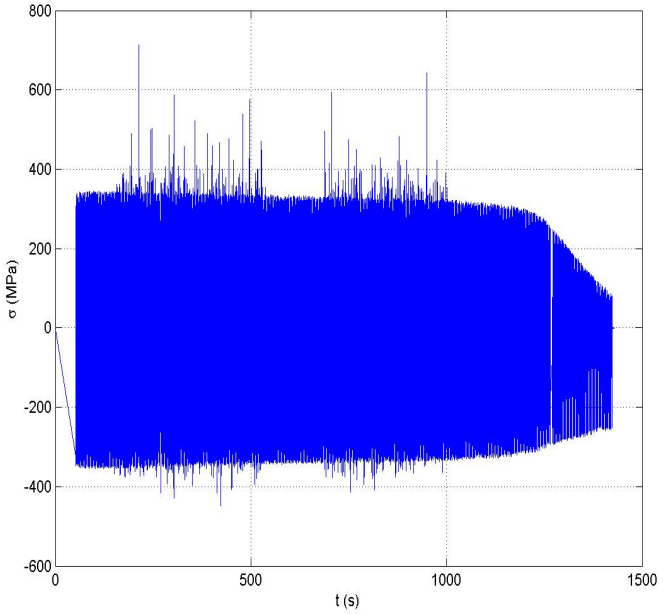

Figure D.59: Stress versus Time

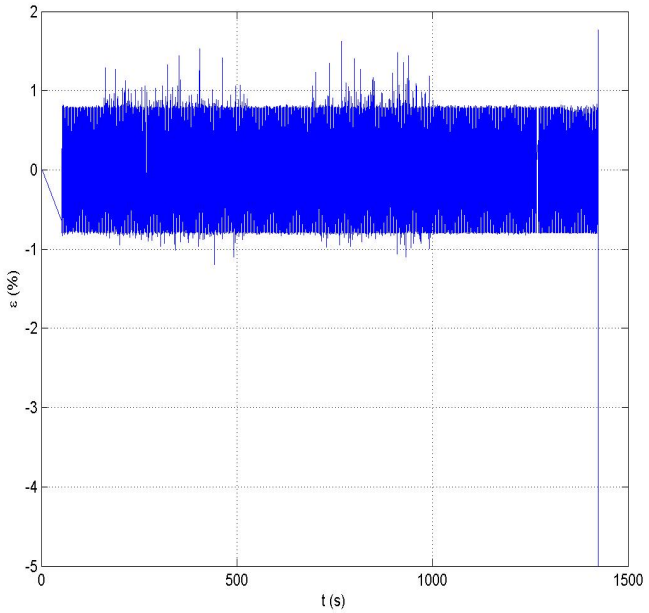

Figure D.60: Strain versus Time

Sample 16

Interferences produced by a static testing machine running close by.

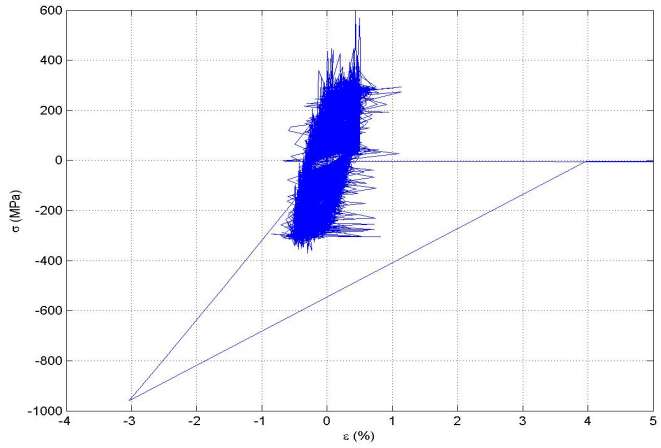

Figure D.61: Hysteresis Curve

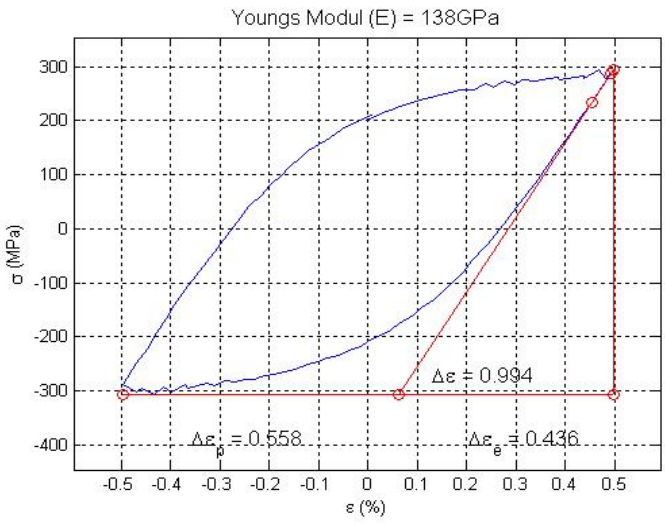

Figure D.62: Hysteresis Curve: Young's Modulus

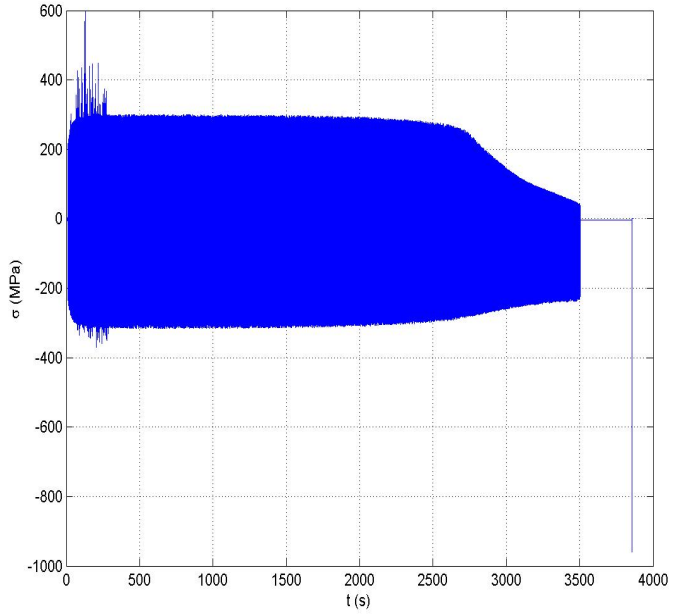

Figure D.63: Stress versus Time

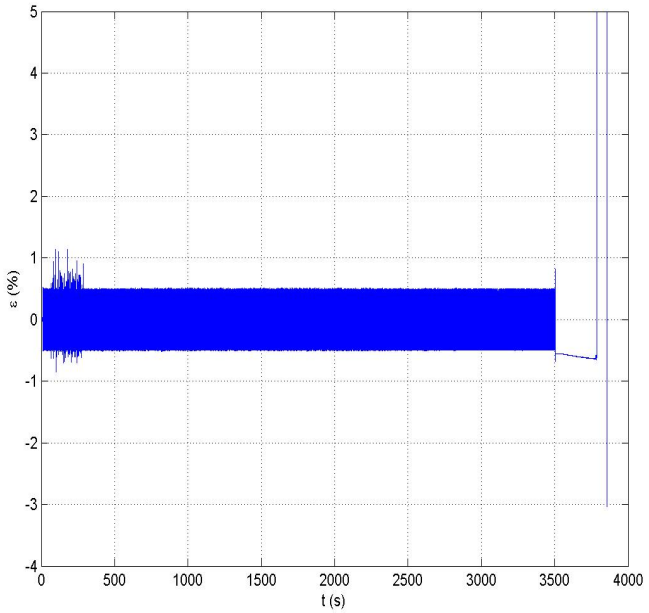

Figure D.64: Strain versus Time